Petroleum Science 23 (2026) 5887–5907

Contents lists available at ScienceDirect

Petroleum Science

journal homepage: www.keaipublishing.com/en/journals/petroleum-science

Original Paper

A low-dimensional dynamic model for slug elimination in pipeline-riser system

Han-Xuan Wang [a], Tian-Yu Liu [a], Sui-Feng Zou [a,*], Jie Sun [b], Lie-Jin Guo [a,**]

[a] State Key Laboratory of Multiphase Flow in Power Engineering, Xi'an Jiaotong University, Xi'an, 710049, Shaanxi, China
[b] School of Oil & Natural Gas Engineering, Southwest Petroleum University, Chengdu, 610500, Sichuan, China

ARTICLE INFO

Article history:
Received 26 May 2025
Received in revised form
14 February 2026
Accepted 9 July 2026
Available online 15 July 2026

Edited by Xi Zhang

Keywords:
Slugging elimination
Pipeline-riser system
Low-dimensional model
Active control

ABSTRACT

A low-dimensional model for slug elimination is established to improve the applicability and accuracy of current models. Inspired by the flow stages of severe slug flow, the model in this paper is divided into three distinct flow stages—slug growth, liquid production, and blowout stages—to accurately capture the flow behaviors of severe slugging flow. For high-pressure operating conditions, a multiphase valve model considering phase slip and critical flow is analyzed and applied to expand the application boundary of the low-dimensional model. The new model and the state-of-the-art low-dimensional model reported in the literature are compared in detail with the results from experiments and the OLGA simulator. The results show that the new model can well simulate the flow behaviors of SS1 and SS2. In the three validation conditions, the absolute values of the mean relative errors of the new (old) model for the simulation of flow cycle, riser pressure drop, and inlet pressure are 2.67% (103.52%), 6.51% (22.88%), and 2.84% (11.31%), respectively.

1. Introduction

In recent years, pipeline-riser systems have experienced rapid development in the offshore oil and gas industry because of the significant advantages in cost-effectiveness and project management (Havre et al., 2000). As shown in Fig. 1, such system generally consists of an undulating pipeline laid on the seabed and a riser connected to the floating production storage and offloading (FPSO). However, due to the unique geometric structure of the pipeline-riser system, a hazardous flow regime known as severe slugging flow may occur under low-production conditions (Yu et al., 2023), typically during the late or early stages of the production cycle.

Severe slugging flow is a global multiphase flow regime (Zou et al., 2017), which exhibits periodic flow behavior accompanied by significant pressure and flow rates fluctuations. Its most typical feature is that it usually consists of several definite flow stages. When severe slugging flow occurs, the flow circulates among these stages, and exhibits different macro flow phenomena, i.e., different severe slugging flow sub-regimes, depending on the flow stages experienced in the cycle. Among them, the most important sub-regimes include Type 1 severe slugging flow (SS1) and Type 2 severe slugging flow (SS2): the former mainly occurs under low gas-liquid velocity conditions, while the latter occurs under conditions with a relatively high gas-liquid ratio.

SS1 is composed of four flow stages (Taitel et al., 1990), namely slug growth, liquid production, blowout, and liquid fallback. During the slug growth stage, as liquid continuously accumulates at the riser base, it blocks the gas passage at the bottom of the riser, thereby preventing gas from entering the riser. This causes gas to accumulate within the pipeline, meanwhile, the lower section of the riser is occupied by pure liquid, while the upper section is filled with gas, which interacts dynamically with the external environment via the outlet valve; during the liquid production stage, the entire riser is filled with liquid driven by the pressurized gas in the pipeline. Concurrently, the gas-liquid interface in the pipeline moves downward toward the riser base. Once the interface reaches the bottom of the riser, the system transitions to the blowout stage; during the blowout stage, gas first enters the riser and undergoes rapid expansion, thereby propelling the liquid to discharge rapidly. Subsequently, the gas thoroughly mixes with

* Corresponding author.
** Corresponding author.
E-mail addresses: zou_suifeng@xjtu.edu.cn (S.-F. Zou), lj-guo@xjtu.edu.cn (L.-J. Guo).
Peer review under the responsibility of China University of Petroleum (Beijing).

https://doi.org/10.1016/j.petsci.2026.07.016
1995-8226/

Nomenclature

A	cross-sectional area,m^2
a	constant, = 0.6152
c	constant, = −0.85
D	diameter, m
f	resistance coefficient
g	gravitational acceleration, m/s^2
H	height of the riser, m
h	liquid level, m
K_v	valve flow coefficient, m^3/h
L	length, m
M	gas molecular, kg/mol
m	mass, Kg
N_{Re}	Reynolds number
n	amount of substance, mol
P	Pressure, Pa
r	radius, m
T	temperature, K
t	time, s
U	velocity, m/s
V	volume, m^3
w	mass flow rate, kg/s
x	volumetric liquid holdup, %
Z	compressibility factor
z	valve opening, %

Greek symbols

α	liquid holdup, %
Δ	ΔP, pressure drop, Pa
ε	pipe roughness, m
θ	pipeline inclination angle, °
μ	viscosity, Pas
π	Pi
ρ	density, kg/m^3
σ	two-phase multiplier
Φ	two-phase friction multiplier
ϕ	angle, °

Subscript

0	standard condition
3	L3
c	critical, h_c
down	downward pipeline
elbow	elbow
f	friction force
G	single-phase gas
g	gas
hor	horizontal pipeline
in	inlet
L	single-phase liquid
l	liquid
mix	mixture
non-blowout	non-blowout stage
out	outlet
pipe	pipeline
riser	riser
S	separator
SL	liquid superficial
travel	L_{travel}, flow length of liquid
valve	valve

the liquid, forming a gas-liquid two-phase flow that erupts from the riser. As a result, the outlet first exhibits a high-velocity outflow of single-phase liquid, which then transitions to the eruption of gas-liquid two-phase flow. If the liquid within the riser is insufficient to sustain the rapid blowout, the flow transitions into the liquid fallback stage. At this time, the gas passage is interconnected from the bottom of the riser to the riser outlet. Meanwhile, the liquid adheres to the inner wall of the riser and flows back towards the bottom of the riser. It then accumulates at the bottom of the riser, re-blocking the gas passage, and the flow enter the next period. The cycle of SS2 only does not include the liquid production stage, and the definitions of the other flow stages are consistent with those of SS1. The detailed flow characteristics and corresponding pressure profile diagrams for the two flow regimes are presented in Fig. 2. In recent decades, researchers have carried out extensive work on the theoretical analysis and stability criteria of severe slugging flow (Cao et al., 2024; Jansen et al., 1996; Liu et al., 2025; Malekzadeh et al., 2012; Taitel, 1986; Taitel et al., 1990; Wang et al., 2026), as well as experimental studies under atmospheric (Li et al., 2017; Yu et al., 2024; Zhou et al., 2018) and high-pressure conditions (Xie et al., 2017; Zhao et al., 2023).

Severe slugging flow can cause substantial and periodic fluctuations in flow rates and pressure, posing a significant threat to the service life of pipelines and the normal operation of downstream production equipment. In extreme cases, it can lead to overflow in downstream separators, forcing the system to shut down and resulting in substantial economic losses (Wang et al., 2024). Therefore, effective methods to suppress or eliminate severe slugging flow are required, which are known as slug elimination technology. For more details on the hazards and elimination techniques of severe slugging, please refer to the reviews (Banjara et al., 2023; Chen et al., 2025; Pedersen et al., 2017).

Among all slug elimination techniques (Banjara et al., 2023; Chen et al., 2025; Pedersen et al., 2017), active feedback control is regarded as a preferred method due to its high efficiency, affordability, and minimal side effects (Havre and Dalsmo, 2002; Jahanshahi and Skogestad, 2011; Nnabuife et al., 2022). The dynamic model of the severe slugging flow serves as the cornerstone of this technology and are frequently applied to the design of controllers (Jahanshahi et al., 2014; Ogazi et al., 2010; Park et al., 2021) and estimators (Wang et al., 2023). Although partial differential equations (PDEs) models (Azevedo et al., 2015; Baliño et al., 2010; Han and Guo, 2015) based on computational fluid dynamics offer higher computational accuracy, they are difficult to apply directly to the design of controllers and estimators, as control theory is primarily established on ordinary differential equations (ODEs). To convert the PDE model into an ODE model, it is necessary to transform the variables at each node into state variables to eliminate the influence of spatial differences. The result is a state-space model of enormous dimensionality, which will continue to increase if the number of nodes grows.

Consequently, researchers have developed low-dimensional dynamic models (Jahanshahi and Skogestad, 2011; Kaasa et al., 2008; Meglio et al., 2009; Storkaas and Skogestad, 2003) that divide the pipeline-riser system into two modules: the “pipeline” and the “riser”, thereby enabling simplified modeling and analysis of the system. Typical low-dimensional models are constructed based on mass conservation relationships both within and

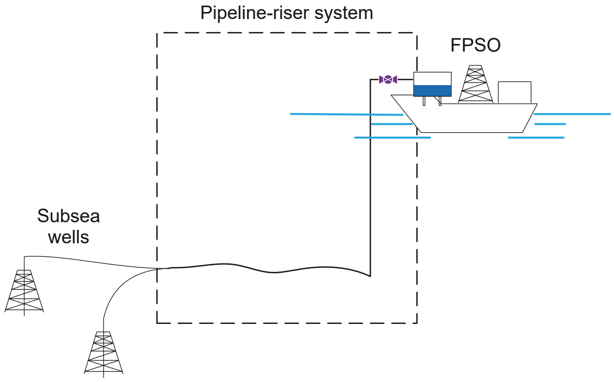

Fig. 1. Schematic diagram of the pipeline-riser system.

between modules. These models are usually described by 3 to 4 state variables, and the system of equations is closed by introducing tunable parameters. Further case studies in controller (Jahanshahi et al., 2014; Ogazi et al., 2010; Park et al., 2021) and estimator design (Wang et al., 2023) have also demonstrated the model's effectiveness in active feedback control, which is why low-dimensional models are often referred to as “control-oriented models”.

However, existing low-dimensional dynamic models still face several challenges, one of which is the parameter tuning process. Such models typically rely on introducing additional tunable parameters to achieve equation closure (as shown in Table 1, the number of tunable parameters ranges from 3 to 7 across different models). The large number of parameters and their strong interdependencies significantly increase the difficulty of tuning (Jahanshahi and Skogestad, 2011). To achieve satisfactory simulation results, operators often need to invest substantial time in parameter adjustment. The second challenge lies in the valve model (Pedersen et al., 2017). Conventional low-dimensional models typically adopt a single-phase valve model (Meglio et al., 2009) or a homogeneous-flow valve model (Jahanshahi and Skogestad, 2011; Storkaas and Skogestad, 2003) to describe valve behavior, both of which neglect fluid compressibility and the effects of critical flow. Although these models perform well under laboratory conditions, they introduce theoretical limitations in industrial field applications—especially under high-pressure conditions where fluid compressibility cannot be ignored, or when valve operates in critical flow. Under such circumstances, the prediction error of incompressible-flow valve models may become non-negligible (Schüller et al., 2006), substantially undermining the reliability of the dynamic model.

To extend the application boundary of the low-dimensional model to high-pressure conditions and industrial sites, a new low-dimensional model was established based on the existing low-dimensional models. To address the challenges posed by high-pressure conditions and large-scale pipeline systems, a multiphase flow valve model (Shao et al., 2018) considering interphase slip and valve critical flow phenomena was introduced. Inspired by the division of flow stages of severe slugging flow, the new model is divided into three flow stages: slug growth, liquid production, and

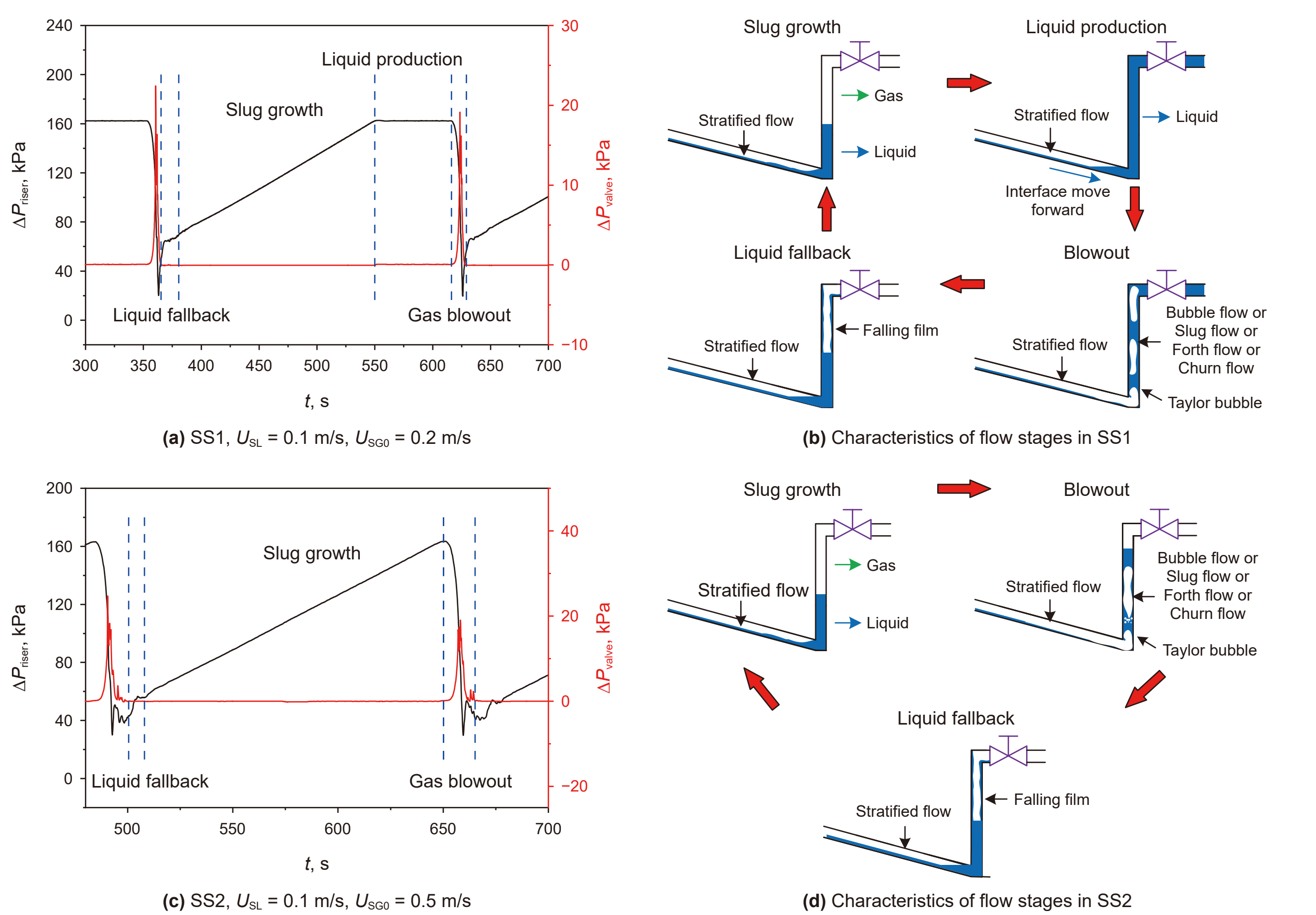

Fig. 2. The detailed flow characteristics of SS1 and SS2.

blowout, so as to accurately simulate the flow behavior of severe slugging flow in different flow stages. For different flow stages, based on the analysis of the flow characteristics of the slugging flow (Cao et al., 2024; Zou et al., 2017, 2021), the new model will adopt different formulas to calculate key parameters such as liquid holdup and pressure drop, thus endowing it with the potential to simulate two severe slugging flow regimes (SS1 and SS2). In addition, through careful evaluation of the tunable parameters of existing models, the number of tunable parameters of the new model was reduced to two, and the parameter tuning process was also discussed in detail to minimize the difficulty of parameter tuning and improve the practicality of the model. The new model, together with the state-of-the-art low-dimensional model (Jahanshahi and Skogestad, 2011) which was termed benchmark model in this paper, is compared with the results from experiments and the OLGA simulator. Two sets of experimental conditions, corresponding to SS1 and SS2 respectively, along with an additional set of simulation condition generated by the OLGA, were selected as the basis for model validation. The simulation results including the bifurcation diagram, pressure and pressure difference parameters, as well as liquid holdup and outlet mass flow rates, are displayed in detail to compare the simulation performance of the new and old models. Finally, the control performance of the controller designed based on the model established in this paper is also demonstrated under three validation conditions.

This paper is organized as follows: Section 2 describes the experimental system used for model validation. Section 3 introduces the model itself and details the parameter tuning process. Section 4 provides a thorough analysis of multiple validation conditions, encompassing both experimental and simulation cases. Finally, Section 5 presents the conclusions.

2. Experimental system

Fig. 3 presents a simple schematic diagram of the test loop employed in this study. The geometric dimensions of the experimental loop and the measurement points for key data are depicted in the figure. The experimental loop consists of a 114 m horizontal pipe, an 18.7 m downward–inclined pipe, and a 16.3 m vertical pipe, followed by an approximately 1.5 m horizontal pipe downstream of the vertical pipe. The pipeline has a downward inclination angle of $-5°$. Both the pipeline and the riser have an inner diameter of 50 mm. Their material is 304 stainless steel, and they are connected by flanges. Consequently, the surface roughness of the inner-wall of the pipeline ranges from 0.025 to 1 μm. The choke valve is installed on the horizontal pipe located downstream of the riser. Prior to conducting the experiment, the flow characteristics of the valve were recalibrated according to the Chinese national standard GB/T 30832–2014.

The working fluid of the experimental system are water and air. For the measurement of liquid phase flow rate, two electromagnetic flowmeters with different measurement ranges are employed. Their ranges and measurement accuracies are 0–6.36 m^3/h with an accuracy of 0.5% F.S. and 0–42.5 m^3/h with an accuracy of 0.5% F.S., respectively. As for the gas-phase flow rate, three orifice flowmeters with different measurement ranges are utilized. Their ranges and measurement accuracies are 1.85–12.9 NL/min with an accuracy of 0.5% F.S., 10.6–105 NL/min with an accuracy of 0.5% F.S., and 89–630 NL/min with an accuracy of 0.5% F.S., respectively. Operators select the appropriate measurement range according to the operating conditions to minimize measurement errors. After being measured, the gas-liquid two phase mixture enters the pipeline in the form as shown in Fig. 3.

The measurement module of the experimental system prioritizes pressure and differential pressure measurements. For pressure measurement, Keller PAA25 absolute pressure sensors are utilized, featuring a measurement range of 500 kPa and an accuracy of $\pm$0.25% F.S. For differential pressure measurement, Rosemont 3051CD3 differential pressure sensors are employed. The measurement ranges of these sensors are dynamically adjusted based on the height difference of the measuring points, while maintaining a consistent accuracy of $\pm$0.15% F.S. across all sensors. The primary measurement data comprise the inlet pressure, the pressure at the bottom of the riser, the pressure drop of the riser, and the pressure drop across the choke valve. For the specific measurement points, please refer to Fig. 3. The NI9189 is chosen as the data acquisition chassis for the test system, with the NI9253 and NI9265 serving as the corresponding acquisition and output cards, respectively.

The following defines the boundary and temperature conditions of the test system: the outlet of the test loop is connected to a cyclone separator, where the gas phase is vented to the atmosphere, resulting in an outlet pressure equivalent to atmospheric pressure. Before the experiment commenced, the opening of the reflux valve in the liquid-phase loop was adjusted to stabilize the pressure upstream of the flowmeter at 1.2 MPa (absolute pressure). Meanwhile, the pressure of the compressor (used for gas-phase supply) was increased to 950 kPa (absolute pressure). At this time, the inlet pressures of both the gas and liquid phases were significantly higher than the system backpressure. Therefore, during the experiment, the inlet flow rate could be regarded as constant. The fluid temperature ranged from 15 °C to 30 °C in the experiments, with temperature variations during the experiment neglected. This simplification is justified as temperature fluctuations are secondary to the pressure and flow variations induced by severe slugging, as documented in Nemoto and Baliño (2012).

3. Model description

This section provides a detailed description of the proposed dynamic model. Specifically, Section 3.1 first elaborates on the specific details of the model and finally introduces its solution procedure; Section 3.2 analyzes the different forms of valve parameters; Section 3.3 discusses the parameter tuning process in detail to reduce the difficulty of tuning.

3.1. Introduction to the model

The model is established based on the mass conservation at the inlet, outlet, and between control volumes. The mass exchange between different parts is constrained by three valves, and four

Table 1
Numbers of tuning parameters in existing low-dimensional models.

	Storkaas model (Storkaas and Skogestad, 2003)	Kaasa model (Kaasa et al., 2008)	Nydal model (Martins et al., 2010)	Meglio model (Meglio et al., 2009)	Jahanshahi model (Jahanshahi and Skogestad, 2011)
Tunable parameters	5	7	3	5	4

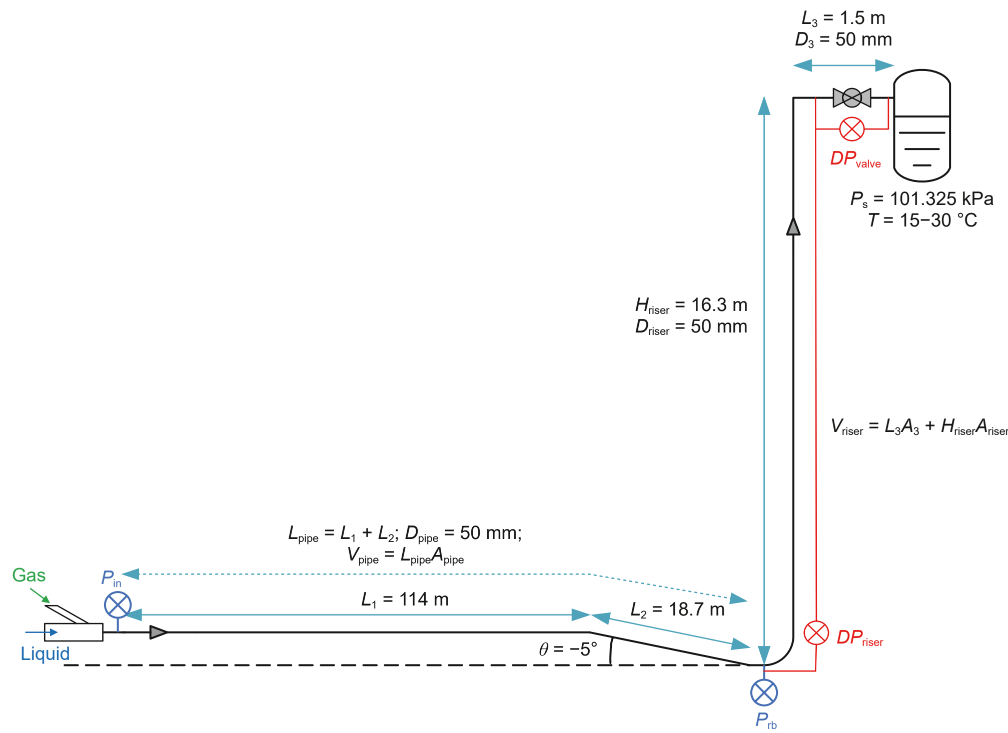

Fig. 3. Schematic diagram of the experimental loop.

appropriate state variables are selected to describe the state information within the system. For detailed information on the control volumes, state variables, and valves, please refer to Table 2 and Fig. 4.

Based on the analysis of the flow characteristics of severe slugging flow, the concept of flow stages is introduced into the low-dimensional model. According to the flow stage classification of severe slugging, the low-dimensional model is divided into two stages: the blowout stage and the non-blowout stage. The non-blowout stage is further subdivided into the slug growth stage and the liquid production stage.

The model first distinguishes between the blowout stage and the non-blowout stage using the equivalent pipeline liquid level height h. The flow is in the blowout stage when h is less than the critical liquid level height h_c, and in the non-blowout stage otherwise, as shown in Eq. (1). The definitions of h and h_c are illustrated in Fig. 5. When the model is in the non-blowout stage, it further distinguishes between the slug growth stage and the liquid production stage based on the liquid mass in the riser $m_{l,riser}$. The flow is in the liquid production stage when the riser (excluding the horizontal pipe downstream of the riser) is fully filled with liquid, and in the slug growth stage otherwise, as shown in Eq. (2).

$$\begin{array}{lll} \text{Blowout,} & \text{if} & h < h_c \\ \text{non}-\text{blowout,} & \text{if} & h \geq h_c \end{array} \tag{1}$$

$$\begin{array}{lll} \text{Slug}-\text{growth,} & \text{if} & V_{l,riser} > = A_{riser}H_{riser} \\ \text{Liquid}-\text{production,} & \text{if} & V_{l,riser} < A_{riser}H_{riser} \end{array} \tag{2}$$

The reason for classifying flow stages in the low-dimensional model is that the multiphase flow regimes inside the control volumes of the “pipeline” and “riser” differ when severe slugging flow is in different flow stages. This results in distinct calculation methods for flow regime-related parameters such as pressure drop and liquid holdup. Conventional low-dimensional models overlook these details. To further improve simulation accuracy, this paper introduces more accurate formulas for liquid holdup and pressure drop based on flow stage classification.

The only exception is the calculation of the liquid holdup α_{pipe} in the control volume “pipeline”. Although a dynamic pipeline liquid holdup α_{pipe} may be a better choice, it was found during simulations that the dynamic pipeline liquid holdup α_{pipe} can lead to numerical instability. Therefore, following the approach of Nemoto and Baliño (2012), the variations in the α_{pipe} are neglected in this study. Jahanshahi and Skogestad (2011) recommended

Table 2
Main parts of the model and their descriptions.

	Name	Description
Control volume	Pipeline	Comprising the horizontal pipe and the downward-inclined pipe.
	Riser	Including the vertical riser and the horizontal pipe downstream of the riser.
Valve	Choke valve	Located at the horizontal pipe section downstream of the riser, it governs the mass exchange between the riser and the external environment.
	Virtual gas valve	Located at the base of the riser, regulates the gas exchange between the pipeline and the riser.
	Virtual liquid valve	Located at the base of the riser, regulates the liquid exchange between the pipeline and the riser.
State variable	$m_{g,pipe}$	Gas mass in pipeline.
	$m_{l,pipe}$	Liquid mass in pipeline.
	$m_{g,riser}$	Gas mass in riser.
	$m_{l,riser}$	Liquid mass in riser.

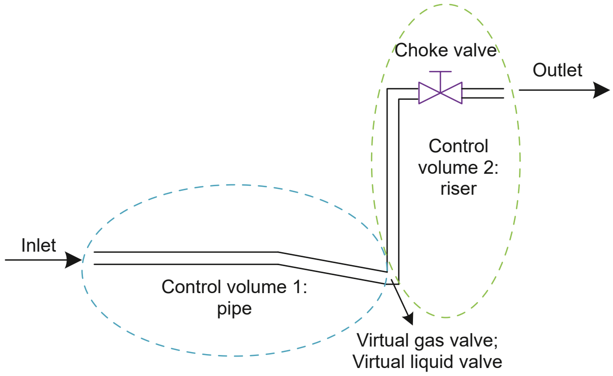

Fig. 4. Schematic diagram of the low-dimensional model.

the use of volumetric liquid holdup for calculations, However, this method introduces considerable errors because it ignores the effects of interphase slip and multiphase flow regimes. Since severe slugging flow occurs only when the flow regime in the pipeline is stratified flow, a more recommended approach is to calculate the α_{pipe} based on stratified flow mechanistic models for horizontal or slightly inclined pipes. Specifically, a slight downward inclination angle can significantly affect the α_{pipe}. For the severe slugging pipeline system consisting of horizontal and downward-inclined pipes, the α_{pipe} is calculated using a weighted average method in this paper, as given in Eq. (3). And the method proposed by Zhou et al. (2002) is adopted to iteratively solve the α_{hor} and α_{down}.

$$\alpha_{\text{pipe}} = (\alpha_{\text{hor}}L_{\text{hor}} + \alpha_{\text{down}}L_{\text{down}}) \Big/ (L_{\text{hor}} + L_{\text{down}}) \tag{3}$$

In this model, it is assumed that the gas satisfies the following conditions (see Eq. (4)).

$$PV = ZnRT \tag{4}$$

Based on fundamental physical laws, the following can be obtained:

$$\begin{aligned} V_{\text{pipe}} &= A_{\text{pipe}}L_{\text{pipe}} \\ V_{\text{riser}} &= A_{\text{riser}}(H_{\text{riser}} + L_3) \end{aligned} \tag{5}$$

$$\begin{aligned} &V_{\text{l,pipe}} = \frac{m_{\text{l,pipe}}}{\rho_{\text{l}}}, V_{\text{l,riser}} = \frac{m_{\text{l,riser}}}{\rho_{\text{l}}} \\ &V_{\text{g,pipe}} = V_{\text{pipe}} - V_{\text{l,pipe}}, V_{\text{g,riser}} = V_{\text{riser}} - V_{\text{l,riser}} \\ &\rho_{\text{g,pipe}} = \frac{m_{\text{g,pipe}}}{V_{\text{g,pipe}}}, \rho_{\text{g,riser}} = \frac{m_{\text{g,riser}}}{V_{\text{g,riser}}} \end{aligned} \tag{6}$$

$$\begin{aligned} P_{\text{in}} &= P_{\text{g,pipe}} = \frac{Zm_{\text{g,pipe}}RT}{MV_{\text{g,pipe}}} \\ P_{\text{out}} &= P_{\text{g,riser}} = \frac{Zm_{\text{g,riser}}RT}{MV_{\text{g,riser}}} \\ \Delta P_{\text{valve}} &= P_{\text{out}} - P_{\text{s}} \end{aligned} \tag{7}$$

$$\begin{aligned} \rho_{\text{mix,pipe}} &= \left(\frac{m_{\text{g,pipe}} + m_{\text{l,pipe}}}{V_{\text{pipe}}}\right) \\ \rho_{\text{mix,riser}} &= \begin{cases} \rho_{\text{l}}, & \text{if} \quad \dfrac{m_{\text{l,riser}}}{\rho_{\text{l}}} >= A_{\text{riser}}H_{\text{riser}} \\ \dfrac{m_{\text{l,riser}} + m_{\text{g,riser}}}{A_{\text{riser}}H_{\text{riser}}}, & \text{if} \quad \dfrac{m_{\text{l,riser}}}{\rho_{\text{l}}} < A_{\text{riser}}H_{\text{riser}} \end{cases} \end{aligned} \tag{8}$$

$$\begin{aligned} U_{\text{mix,pipe}} &= U_{\text{SL}} + U_{\text{SG0}}\frac{\rho_{\text{g0}}}{\rho_{\text{g,pipe}}} = U_{\text{SL,pipe}} + U_{\text{SG,pipe}} \\ U_{\text{mix,riser}} &= U_{\text{SL}}\frac{A_{\text{pipe}}}{A_{\text{riser}}} + U_{\text{SG0}}\frac{\rho_{\text{g0}}A_{\text{pipe}}}{\rho_{\text{g,riser}}A_{\text{riser}}} = U_{\text{SL,riser}} + U_{\text{SG,riser}} \end{aligned} \tag{9}$$

It should be noted that although no subscript is added to the temperature symbol in Eq. (7) for distinction, either the local temperature with higher accuracy or the temperature at the separator can be adopted for calculation.

The critical liquid level h_{c} is determined by Eq. (10), while the liquid level h is calculated based on the state variable $m_{l\text{,pipe}}$ and the geometric model illustrated in Fig. 6, as shown in Eq. (11).

$$h_{\text{c}} = D_{\text{riser}} \tag{10}$$

$$\begin{aligned} m_{\text{l,pipe}} &= \left[\left(L_{\text{pipe}} - \frac{h}{\sin(\theta)}\right)\alpha_{\text{pipe}} + \frac{h}{\sin(\theta)}\right]\rho_{\text{l}}A_{\text{pipe}} \\ h &= \sin(\theta)\frac{m_{\text{l,pipe}}\big/\rho_{\text{l}}A_{\text{pipe}} - L_{\text{pipe}}\alpha_{\text{pipe}}}{\left(1 - \alpha_{\text{pipe}}\right)} \end{aligned} \tag{11}$$

The liquid holdup at the riser base α_{rb} is determined according to the geometry shown in Fig. 6(a), and it can be solved by Eqs. (12) and (13) when h is smaller than h_{c}; otherwise, it equals 1.

$$\begin{aligned} A_{\text{g}} &= 0.25D_{\text{riser}}^2[\pi - \phi - \cos(\pi - \phi)\sin(\pi - \phi)] \\ \phi &= \pi - \arccos\left(1 - \frac{h_{\text{c}} - h}{r_{\text{riser}}}\right) \\ A_{\text{l}} &= A_{\text{riser}} - A_{\text{g}} \end{aligned} \tag{12}$$

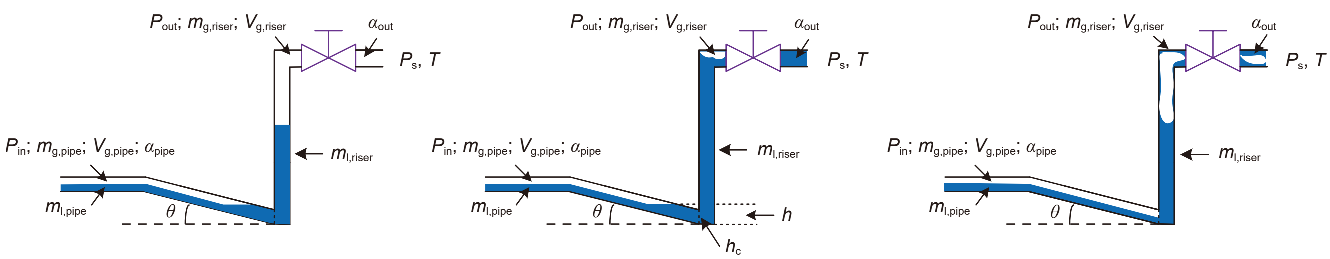

(a) Slug growth (b) Liquid production (c) Blowout

Fig. 5. Classification of flow stages in the model.

$$\alpha_{\mathrm{rb}} = \frac{A_{\mathrm{l}}}{A_{\mathrm{riser}}} \tag{13}$$

The frictional pressure drop in the "pipeline" and "riser" is then calculated based on the identified flow stage, as its determination directly depends on the flow regime.

Regardless of the flow stage in which the model operates, the pressure drop inside the "pipeline" is recommended to be calculated using the stratified flow model. In addition, although the mechanistic model for stratified flow can be used to solve the pressure drop, it requires an iterative procedure that significantly increases the time complexity of the model. Therefore, the pressure drop correlation for stratified flow in horizontal or slightly inclined pipes (Liu et al., 2019) is suggested herein, as detailed in Eqs. (14)–(18).

$$\left(\frac{\mathrm{d}P}{\mathrm{d}z}\right) = \phi^2 \left(\frac{\mathrm{d}P}{\mathrm{d}z}\right)_{\mathrm{L}}, \Delta P_{f,\mathrm{pipe}} = \left(\frac{\mathrm{d}P}{\mathrm{d}z}\right)\left(L_{\mathrm{pipe}}\right) \tag{14}$$

$$\begin{aligned} \phi^2 &= 1 + \frac{C}{X} + \frac{C}{X^2} \\ C &= 1.025 (N_{\mathrm{Re}})_{\mathrm{L}}^{0.517} (N_{\mathrm{Re}})_{\mathrm{G}}^{0.431} \Big/ 1000 \\ X &= \frac{\left(\mathrm{d}P/\mathrm{d}z\right)_{\mathrm{L}}}{\left(\mathrm{d}P/\mathrm{d}z\right)_{\mathrm{G}}} \end{aligned} \tag{15}$$

$$(N_{\mathrm{Re}})_{\mathrm{L}} = \frac{\rho_{\mathrm{l}} U_{\mathrm{SL}} D_{\mathrm{pipe}}}{\mu_l}, (N_{\mathrm{Re}})_{\mathrm{G}} = \frac{\rho_{\mathrm{g,pipe}} U_{\mathrm{SG,pipe}} D_{\mathrm{pipe}}}{\mu_{\mathrm{g}}} \tag{16}$$

The resistance coefficient for stratified flow in horizontal pipes needs to be estimated based on the single-phase (gas and liquid) resistance coefficient. The resistance coefficient of single-phase flow is determined by the Colebrook-White (Colebrook, 1939) formula recommended by Haaland (1983), namely:

$$\frac{1}{\sqrt{f}} = -1.8 \log_{10}\left[\left(\frac{\varepsilon / D_{\mathrm{pipe}}}{3.7}\right)^{1.1} + \frac{6.9}{(N_{\mathrm{Re}})}\right] \tag{17}$$

$$\left(\frac{dP}{dZ}\right)_{\mathrm{L,G}} = \frac{f_{\mathrm{L,G}} \rho_{\mathrm{l,g}} \left(U_{\mathrm{SL,SG}}\right)^2}{2 D_{\mathrm{pipe}}} \tag{18}$$

The calculation method for the pressure drop in the "riser" is slightly different. When the flow is in the slug growth stage, the lower part of the riser is occupied by a pure liquid slug, while the upper part is pure gas. Both liquid and gas are driven by the incoming liquid from the pipeline, so the flow inside the riser is a combination of pure liquid and pure gas flow. When the flow enters the liquid production stage, the liquid slug in the lower part of the riser fills the entire riser and is driven by the incoming liquid from the pipeline too, resulting in pure liquid flow in the "riser". Neglecting the pure gas flow in the riser during the slug growth stage, the flow in the riser can be regarded as pure liquid flow throughout the non-blowout stage, with its flow velocity related to the flow conditions in the "pipeline".

Therefore, it is recommended to use Eq. (17) to calculate the friction coefficient, Eq. (19) to calculate the Reynolds number, and Eq. (20) to calculate the travel distance of the liquid.

$$(N_{\mathrm{Re}})_{\mathrm{riser,non-blowout}} = \frac{\rho_l \left(U_{\mathrm{mix,pipe}} \frac{A_{\mathrm{pipe}}}{A_{\mathrm{riser}}}\right) D_{\mathrm{riser}}}{\mu_{\mathrm{l}}} \tag{19}$$

$$L_{\mathrm{travel}} = \begin{cases} H_{\mathrm{riser}}, & \text{if} \quad \dfrac{M_{\mathrm{l,riser}}}{\rho_{\mathrm{l}} A_{\mathrm{riser}}} > = H_{\mathrm{riser}} \\ \dfrac{m_{\mathrm{l,riser}}}{\rho_{\mathrm{l}} A_{\mathrm{riser}}}, & \text{if} \quad \dfrac{M_{\mathrm{l,riser}}}{\rho_{\mathrm{l}} A_{\mathrm{riser}}} < H_{\mathrm{riser}} \end{cases} \tag{20}$$

For the blowout stage, depending on the operating conditions, the flow regime in the "riser" may manifest as bubbly, slug, churn, or annular flow. The authors attempted to calculate the pressure drop in the "riser" using the slug flow model and achieved satisfactory results. However, the slug flow model has a relatively high computational complexity, which usually involves 1 to 2 iterative procedures: the slug liquid holdup is first solved directly or iteratively based on experimentally fitted correlations (the first iteration); subsequently, other parameters of the slug unit are solved iteratively according to the slug liquid holdup (the second iteration), and the pressure drop of the slug unit is finally determined.

To simplify the calculation, it is recommended to use the frictional pressure drop correlation for bubbly flow—specifically, the Dukler method (Taitel and Dukler, 1976)— to estimate the frictional pressure drop in the "riser" during the blowout stage. The Dukler method is derived based on the homogeneous flow assumption and is suitable for calculating the frictional pressure drop of bubbly flow, as detailed in Eqs. (21)–(24).

$$f_{\mathrm{riser,blowout}} = 0.0056 + 0.5 (N_{\mathrm{Re}})_{\mathrm{riser,blowout}}^{-0.32} \tag{21}$$

$$(N_{\mathrm{Re}})_{\mathrm{riser,blowout}} = \frac{\rho_{\mathrm{mix,riser}} U_{\mathrm{mix,riser}} D_{\mathrm{riser}}}{\mu_{\mathrm{mix,riser}}} \tag{22}$$

$$\mu_{\mathrm{mix,riser}} = \alpha_{\mathrm{riser}} \mu_{\mathrm{l}} + (1 - \alpha_{\mathrm{riser}}) \mu_{\mathrm{g}} \tag{23}$$

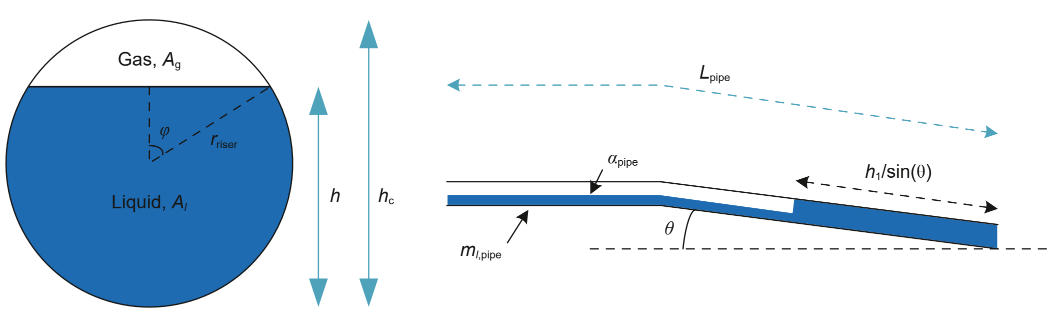

(a) Liquid level and critical liquid level **(b)** Pipeline liquid mass distribution

Fig. 6. Simple geometric structure of the model.

$$\Delta P_{f,\text{riser}} = \frac{f_{\text{riser}}\rho_{\text{mix,riser}}\left(U_{\text{mix,riser}}\right)^2}{2D_{\text{riser}}}\left(H_{\text{riser}} + L_3\right) \tag{24}$$

The liquid holdup in the riser α_{riser} is determined using Eq. (25).

$$\alpha_{\text{riser}} = \begin{cases} 1, & \textit{if} \quad \dfrac{m_{\text{l,riser}}}{\rho_{\text{l}}} >= A_{\text{riser}}H_{\text{riser}} \\ \dfrac{m_{\text{l,riser}}}{\rho_{\text{l}}V_{\text{riser}}}, & \textit{if} \quad \dfrac{m_{\text{l,riser}}}{\rho_{\text{l}}} < A_{\text{riser}}H_{\text{riser}} \end{cases} \tag{25}$$

After calculating the frictional pressure drop for each control volume, the pressure drops across the virtual liquid-phase (and gas-phase) valve can be determined using Eqs. (26–27). These parameters govern the mass transfer between the "pipeline" and the "riser."

$$\begin{aligned}\Delta P_{\text{l,rb}} = &\left(P_{\text{in}} - \Delta P_{f,\text{pipe}} + \rho_{\text{l}}gh_1\right) \\ &- \left(P_{\text{out}} + \rho_{\text{mix,riser}}gH_{\text{riser}} + \Delta P_{f,\text{riser}}\right)\end{aligned} \tag{26}$$

$$\begin{aligned}\Delta P_{\text{g,rb}} = &\left(P_{\text{in}} - \Delta P_{f,\text{pipe}}\right) \\ &- \left[P_{\text{out}} + \rho_{\text{mix,riser}}g(H_{\text{riser}} - D_{\text{riser}}) + \Delta P_{f,\text{riser}}\right]\end{aligned} \tag{27}$$

For the mass exchange between the pipeline and the riser, it is assumed to be governed by two virtual valves; in addition, since the pressure drop of the gas valve determined by Eq. (26) is extremely small, the compressibility of the gas can be neglected. Therefore, it is recommended to use Eqs. (27) and (28) to calculate the mass exchange between the "pipeline" and the "riser." During the non-blowout stage, A_{g} equals zero, resulting in no substantial gas mass transfer. This implies that gas is forced to accumulate within the "pipeline." It should be emphasized that using virtual valves to calculate the mass exchange between the "riser" and the "pipeline" is a common method for low-dimensional models, but not the only one—the PDE model (Andreolli et al., 2018; Baliño et al., 2010) uses the drift flux model to calculate the corresponding mass exchange.

$$\begin{aligned} U_{\text{g,rb}} &= \sqrt{\max\left(0, \frac{\Delta P_{\text{g,rb}}}{\rho_{\text{g,pipe}}f_{\text{g}}}\right)} \\ U_{\text{l,rb}} &= \operatorname{sgn}\left(\Delta P_{\text{l,rb}}\right)\sqrt{\operatorname{abs}\left(\frac{\Delta P_{\text{l,rb}}}{\rho_{\text{l}}f_{\text{l}}}\right)} \end{aligned} \tag{28}$$

$$\begin{aligned} w_{\text{g,rb}} &= U_{\text{g,rb}}A_{\text{g}}\rho_{\text{g,pipe}} \\ w_{\text{l,rb}} &= U_{\text{l,rb}}A_{\text{l}}\rho_{\text{l}} \end{aligned} \tag{29}$$

Additionally, please note that the sgn(), abs(), and max() functions in Eq. (28) are crucial for the stable operation of the calculation and cannot be omitted. These operations dictate the direction of mass exchange: at the bottom of the riser, liquid is allowed to flow back into the pipeline, while gas is prevented from flowing back into the pipeline.

The mass exchange of the outlet valve is much more complicated than that of the virtual valves at the bottom of the riser, which needs to be explained in detail. For the non-blowout stage, the valve operates in a single-phase condition. Simply put, during the slug growth stage, only gas passes through the valve, and the pressure drop is very small and almost negligible. Therefore, a single-phase incompressible flow valve model can be adopted, as shown in Eqs. (30) and (31). During the liquid production stage, only liquid flows out of the valve, and the single-phase incompressible flow valve model is also adopted, as shown in Eqs. (32) and (33). The only difference between the two is that the valve allows gas to flow back into the riser, but does not allow liquid to flow back, which is exactly the opposite of the situation at the bottom of the riser.

$$U_{\text{g,out}} = \operatorname{sgn}(\Delta P_{\text{valve}})\sqrt{\operatorname{abs}\left(\frac{\Delta P_{\text{valve}}}{\rho_{\text{g,riser}}f_{\text{valve}}}\right)} \tag{30}$$

$$\begin{aligned} w_{\text{g,out}} &= \rho_{\text{g,riser}}U_{\text{g,out}}A_{\text{riser}} \\ w_{\text{l,out}} &= 0 \end{aligned} \tag{31}$$

$$U_{\text{l,out}} = \sqrt{\max\left(0, \frac{\Delta P_{\text{valve}}}{\rho_{\text{l}}f_{\text{valve}}}\right)} \tag{32}$$

$$\begin{aligned} w_{\text{l,out}} &= \rho_{\text{l}}U_{\text{l,out}}A_{\text{riser}} \\ w_{\text{g,out}} &= 0 \end{aligned} \tag{33}$$

During the blowout stage, although the actual fluid passing through the valve initially consists of high-speed single-phase liquid followed by gas–liquid two-phase flow, researchers conventionally neglect the single-phase liquid flow and develop both PDE (Andreolli et al., 2018; Azevedo et al., 2015; Azevedo et al., 2017) and ODE models (Jahanshahi and Skogestad, 2011; Meglio et al., 2009; Storkaas and Skogestad, 2003) based on a homogeneous flow valve model, which have achieved satisfactory simulation results. Additionally, Meglio et al. (2009) suggests using a single-phase flow valve model for modeling, which has also achieved good simulation results.

Therefore, the authors compared the single-phase flow valve model, the homogeneous flow valve model, and a modified homogeneous flow model incorporating with two-phase multiplier (Wang et al., 2026). The results demonstrate that the modified homogeneous flow model provides the best agreement over the entire flow range and also requires the least effort in parameter adjustment, as detailed in Eqs. (34)–(39).

$$\Delta \text{P}_{\text{valve}} = f_{\text{valve}}\sigma\rho_{\text{mix,out}}U_{\text{mix,out}}{}^2 \tag{34}$$

$$\sigma = e^{a\frac{U_{\text{SL,riser}}}{U_{\text{mix,riser}}}} + c \tag{35}$$

The values of a and c are 0.6152 and −0.85, respectively.

$$U_{\text{mix,out}} = \operatorname{sgn}(\Delta P_{\text{valve}})\sqrt{\frac{\operatorname{abs}(\Delta P_{\text{valve}})}{f_{\text{valve}}\varepsilon\rho_{\text{mix,out}}}} \tag{36}$$

$$x_{\text{l,out}} = \frac{\alpha_{\text{out}}\rho_{\text{l}}}{\alpha_{\text{out}}\rho_{\text{l}} + (1 - \alpha_{\text{out}})\rho_{\text{g,riser}}} \tag{37}$$

$$U_{\text{mix,out}} = \rho_{\text{mix,out}}A_{\text{riser}}u_{\text{mix,out}} \tag{38}$$

$$\begin{aligned} w_{\text{l,out}} &= \max\left(0, \rho_{\text{mix,out}}A_{\text{riser}}U_{\text{mix,out}}x_{\text{l,out}}\right) \\ w_{\text{g,out}} &= w_{\text{mix,out}} - w_{\text{l,out}} \end{aligned} \tag{39}$$

However, both the homogeneous flow model and the single-phase flow model actually neglect the compressibility of the gas phase, thereby introducing calculation errors (Schüller et al., 2006). For industrial sites as well as high-pressure and long-distance pipelines, the use of a multiphase flow valve model may be a better choice (Pedersen et al., 2017). Therefore, this paper attempts to introduce a multiphase flow valve model to replace the traditional incompressible flow valve model, with specific details provided in Appendix A.

Established on the basis of Alsafran and Kelkar (2007), this multiphase flow valve model (Shao et al., 2018) considers interphase slip and assumes that the gas is in adiabatic flow; during the calculation, it is necessary to first calculate the critical pressure ratio through an iterative process to determine the valve flow regime.

Based on the flow characteristic analysis, the liquid holdup at the outlet [α_{out}] is determined by a discontinuous piecewise function according to flow stages. For the blowout stage, Jahanshahi's form is still used, see Eq. (40), which performs well in the blowout stage but has a large error in the non-blowout stage.

$$\alpha_{\text{out}} = \begin{cases} \alpha_{\text{riser}}, & \text{if} \quad \alpha_{\text{rb}} \le \alpha_{\text{riser}} \\ 2\alpha_{\text{riser}} - \alpha_{\text{rb}}, & \text{if} \quad \alpha_{\text{riser}} < \alpha_{\text{rb}} \le 2\alpha_{\text{riser}} \\ 0, & \text{if} \quad \alpha_{\text{rb}} \ge 2\alpha_{\text{riser}} \end{cases} \tag{40}$$

For the non-blowout stage, a simple formula is used to determine the α_{out}, see Eq. (41). Compared with the formula for calculating the liquid holdup at the outlet in the established models, the easy formula for the α_{out} which is built based on the flow characteristic analysis of slugging flow gives the model a better performance without adding tunable parameters, which will be specifically discussed in Section 4.

$$\alpha_{\text{out}} = \begin{cases} 0, & \text{if} \quad \text{slug} - \text{growth} \\ 1, & \text{if} \quad \text{liquid} - \text{production} \end{cases} \tag{41}$$

Finally, based on the law of mass conservation, the state transition equations for the state variables are derived as follows:

$$\dot{m}_{\text{g,pipe}} = \frac{\mathrm{d}m_{\text{g,pipe}}}{\mathrm{d}t} = w_{\text{g,in}} - w_{\text{g,rb}} \tag{42}$$

$$\dot{m}_{\text{l,pipe}} = \frac{\mathrm{d}m_{\text{l,pipe}}}{\mathrm{d}t} = w_{\text{l,in}} - w_{\text{l,rb}} \tag{43}$$

$$\dot{m}_{\text{g,riser}} = \frac{\mathrm{d}m_{\text{g,riser}}}{\mathrm{d}t} = w_{\text{g,rb}} - w_{\text{g,out}} \tag{44}$$

$$\dot{m}_{\text{l,riser}} = \frac{\mathrm{d}m_{\text{l,riser}}}{\mathrm{d}t} = w_{\text{l,rb}} - w_{\text{l,out}} \tag{45}$$

The basic solution procedure of the model in this paper is as follows: first, all relevant parameters at the same time step are calculated based on the state variables, and then the state variables at the next time step are solved based on the state transition equations to complete the entire solution procedure. The complete computational flowchart of the model is shown in Fig. 7.

3.2. Discussion on valve parameters

Valve parameters are core parameters for measuring the throttling capacity of valves and are used to quantitatively describe valves in the model. Since the valve opening itself cannot directly represent its throttling capacity, it is necessary to clarify the corresponding relationship between valve parameters and valve opening, thereby converting the valve opening into quantifiable throttling capacity.

For the incompressible flow valve model (including homogeneous flow valves and single-phase flow valves), this paper uses the valve resistance coefficient f_{valve} as the valve parameter to quantitatively characterize the throttling capacity of the valve, and its corresponding relationship with the valve flow coefficient K_{v} is shown in Eq. (46). Based on Eq. (46) and the valve flow characteristic curve (i.e., the K_{v} - z relationship), when the inner diameter of the pipeline where the valve is installed is known, a clear corresponding relationship between f_{valve} and z can be established. It should be emphasized that A_{riser} in Eq. (46) is the cross-sectional area of the pipeline where the valve is installed; therefore, when

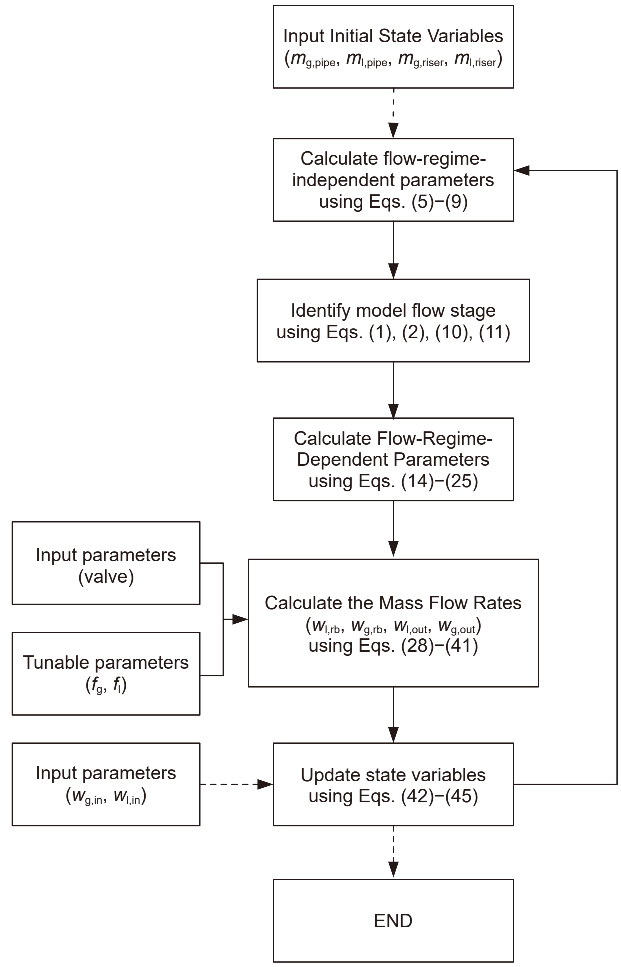

Fig. 7. Schematic diagram of the proposed model's computational workflow.

the same valve is installed in different pipelines, the corresponding relationship between its resistance coefficient f_{valve} and valve opening z will also be different.

For the multiphase flow valve model, the equivalent throttling orifice diameter D_{valve} is usually used to characterize the throttling capacity of the valve. Therefore, to apply the multiphase flow valve model, it is necessary to clarify the corresponding relationship between D_{valve} and valve opening, so as to realize the quantitative description of the valve in the model under different openings. By defining the valve coefficient C_{d}, the correlation between the equivalent throttling orifice diameter D_{valve} and the flow coefficient K_{v} can be established. Assuming that C_{d} remains constant, the corresponding relationship between D_{valve} and K_{v} can be solved, and please refer to Appendix A for details.

Therefore, for the above two valve models, the valve parameters are actually correlated with the flow coefficient K_{v} to obtain their corresponding relationship with the valve opening. The valve flow characteristic curve is usually provided by the valve manufacturer, but it is recommended that, when experimental conditions are available, engineers should conduct pure water experiments in accordance with relevant standards to obtain more accurate flow characteristic curves (Schüller et al., 2006).

$$f_{\text{valve}} = \frac{(36000A_{\text{riser}})^2}{{K_{\text{v}}}^2} \tag{46}$$

The above process has discussed how to establish the corresponding relationship between valve parameters and valve

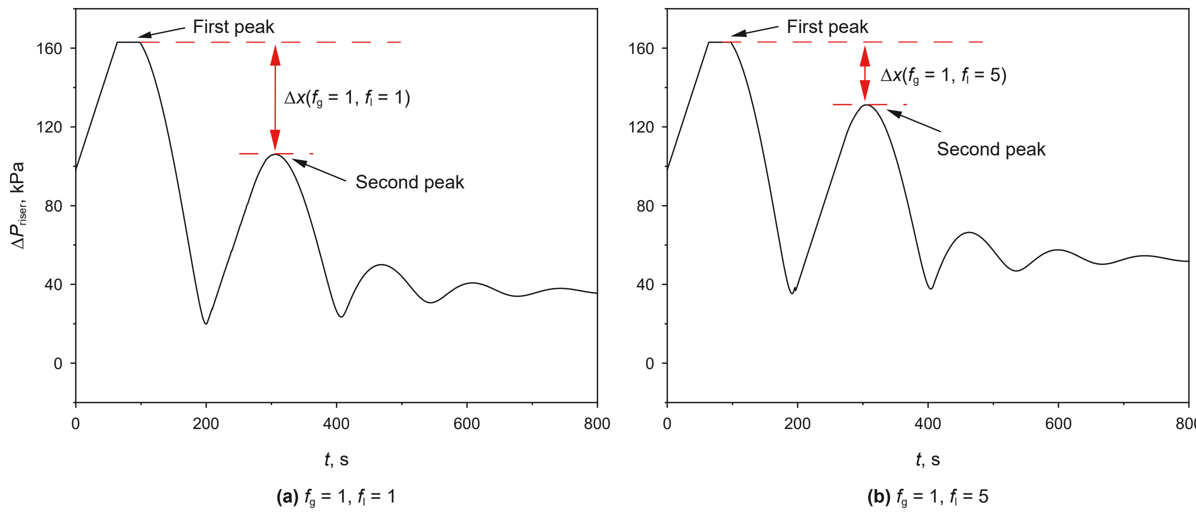

Fig. 8. Demonstration of the method for judging model stability. ($\boldsymbol{U}_{SL} = 0.1$ m/s, $\boldsymbol{U}_{SG0} = 0.5$ m/s, $f_{valve} = 1506.76$).

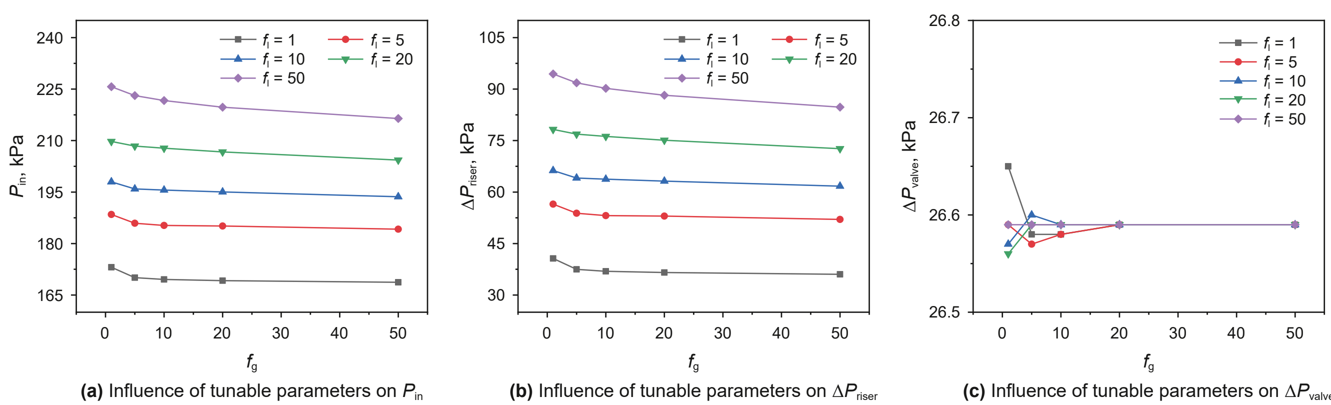

Fig. 9. Demonstration of the influence of tunable parameters on stable state parameters. ($\boldsymbol{U}_{SL} = 0.1$ m/s, $\boldsymbol{U}_{SG0} = 0.5$ m/s, $f_{valve} = 2000$).

opening. However, low-dimensional models need to undergo local linearization to obtain a linear state-space model, and the specific linearization process can be referred to in the literature (Ogazi et al., 2010). Therefore, to realize this linearization process, it is necessary to define the functional relationship between valve parameters and valve opening, rather than a simple corresponding relationship. Traditional low-dimensional models suggest assuming that the valve has linear flow characteristics to further determine the functional relationship between the two; according to the results of relevant literature (Jahanshahi and Skogestad, 2011; Meglio et al., 2009), although this method introduces a certain degree of calculation error, it is acceptable overall.

3.3. Model parameter tuning

Low-dimensional models achieve the closure of the equation system by introducing tunable parameters, and parameter tuning is the process of adjusting these tunable parameters to enable the low-dimensional model to accurately simulate the flow system. Obviously, low-dimensional models cannot achieve perfect simulation of the flow system; therefore, clarifying the evaluation criteria for simulation performance and establishing a reasonable parameter tuning process are crucial for reducing the difficulty of parameter tuning and improving tuning efficiency. This section will focus on a detailed discussion of tunable parameters, evaluation criteria, and parameter tuning methods.

As shown in Fig. 7, f_g and f_l are the only two tunable parameters in this model, describing the flow capacity of gas and liquid at the riser bottom, respectively. Based on their physical meanings, their definition domains can be estimated in advance. Specifically, f_l can be regarded as the sum of the resistance coefficient of a valve with a diameter approximately equal to the pipeline diameter (the pipeline where the valve is installed) and the resistance coefficient introduced by the elbow, and f_g can be regarded as the sum of the resistance coefficient of a valve with a diameter smaller than the pipeline diameter and the resistance coefficient introduced by the elbow. Therefore, for the pipeline used in the experiments of this paper, it is recommended that the tunable parameters be adjusted within the range specified by Eq. (47).

$$f_g \in [1, 50000], f_l \in [1, 5000] \tag{47}$$

The primary requirement for parameter tuning is to match the critical valve parameters of the flow system, which means the model should accurately simulate the variation trend of the flow system's stability with the valve's throttling capacity. While conventional low-dimensional models rely on matching the critical opening—usually by assuming linear valve flow characteristics and treating $K_{v,max}$ as a tunable parameter—this mapping introduces model mismatch risks, as accurate opening matching does not guarantee accuracy in the critical throttling capacity. Therefore, to avoid the above risk, the model in this paper further requires matching the critical resistance coefficient or the critical

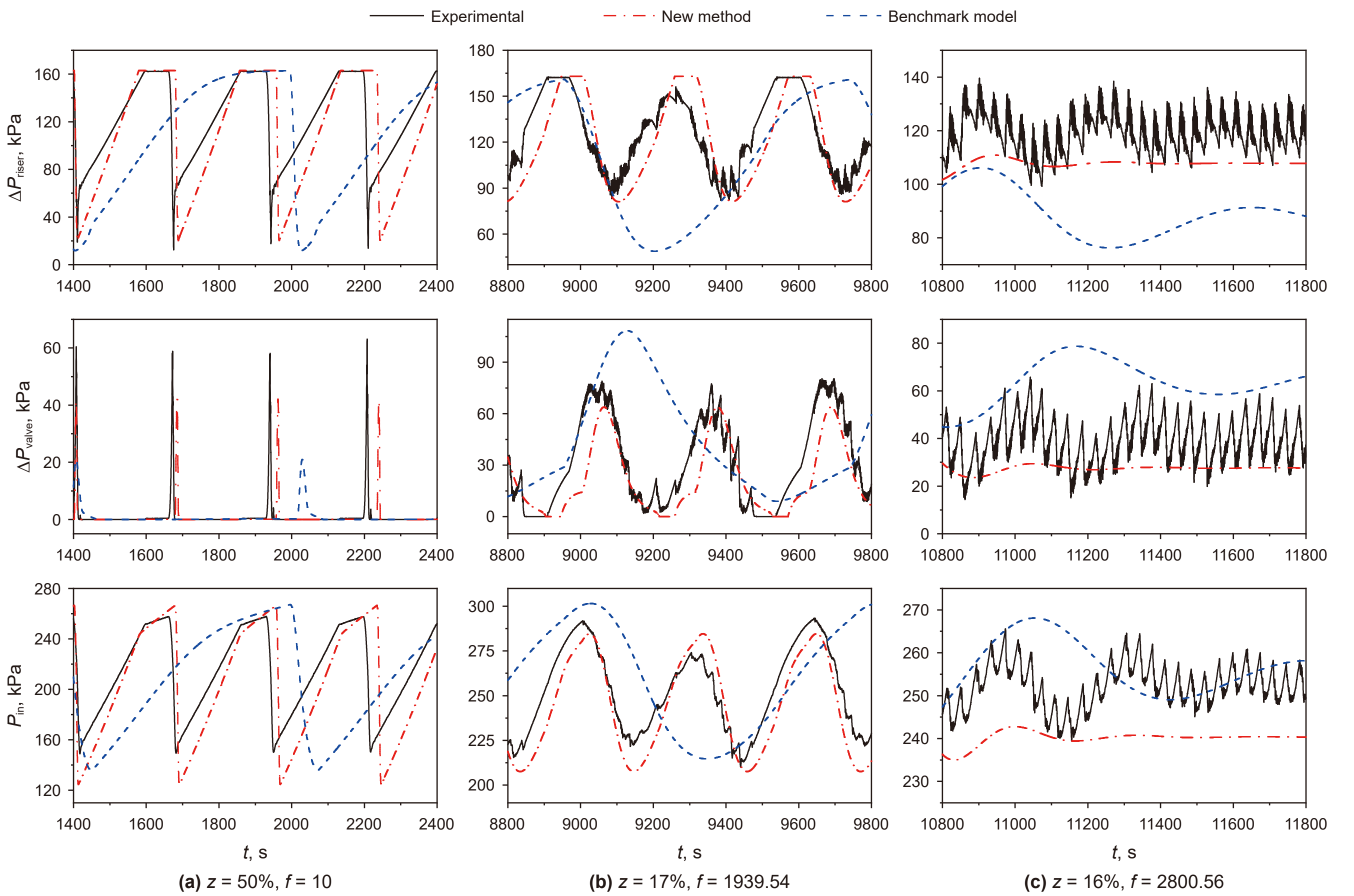

Fig. 10. The micro-display of Case one.

Table 3
Information on parameters required for experimental verification calculation.

Symbol	Description	Value	Unit
g	gravitational acceleration	9.8	m/s^2
R	Universal gas constant	8.314	J/(mol·K)
M	Gas molecular	28.9634e-3	kg/mol
T	Temperature	293.15	K
Z	Compressibility factor	1	·
μ_l	Liquid viscosity	1002e-6	Pa·s
μ_g	Gas viscosity	18.1e-6	Pa·s
ε	Pipe roughness	2.5e-8	m
ρ_l	Liquid density	998.2	kg/m^3
ρ_{g0}	Gas density under standard conditions	1.293	kg/m^3

equivalent throttling orifice diameter. In addition, since local linearization relies on the state variables at the equilibrium point—namely, those corresponding to the critically stable state—the simulation accuracy of flow parameters under this condition serves as a key metric for parameter tuning. In fact, even if stability matching is achieved, excessive deviations in the flow parameters of the stable state will still affect the subsequent local linearization process, thereby interfering with the controller design work.

In summary, the primary task of the parameter tuning process is to adjust the tunable parameters to make the stability of the model consistent with the experimental data. During the parameter tuning process, the operator needs to quickly judge the impact of the current tunable parameters on the model stability, and then determine the rationality of the current parameter adjustment direction. However, such rapid judgment is difficult because stability is an evaluation index lacking quantitative description, making it hard to determine which of the two unstable model operating conditions is more unstable.

To this end, this paper provides a simple method for quickly judging the development trend of model stability. As shown in Fig. 8, the development trend of model stability can be judged by comparing the numerical differences in the peak positions of the

Table 4
Key parameters including slug period of Case one.

	Slug period ($z = 50\%$), s	Slug period ($z = 17\%$), s	ΔP_{riser} ($z = 16\%$), kPa	ΔP_{valve} ($z = 16\%$), kPa	P_{in} ($z = 16\%$), kPa
Experimental results	264.8	318.85	118.76	39.32	252.26
This method	276.84	312.03	108.07	27.62	240.37
Benchmark model	621.39	790.29	86.00	64.78	254.64

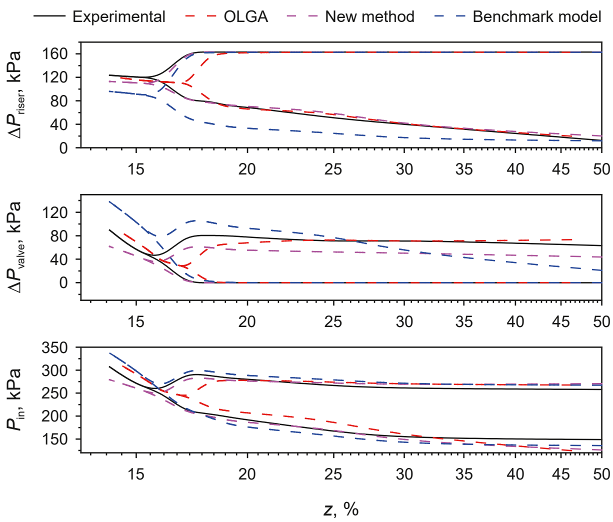

Fig. 11. The bifurcation diagram of Case one.

riser pressure drop: when the difference increases, it indicates that the stability of the model is increasing; on the contrary, when the difference decreases, it indicates that the stability of the model is decreasing.

In the stability matching process, it is necessary to first fix one of the tunable parameters, adjust the other tunable parameter, and find the parameter combination with the optimal model stability within the neighborhood of this tunable parameter; then swap the adjustment order of the two tunable parameters, repeat the above operation process, and finally achieve accurate matching between the model stability and the experimental data.

After completing the matching between the model stability and the experimental data, the tunable parameters can be fine-tuned to further improve the simulation accuracy of each flow parameter in the stable state of the flow system. Fig. 9 shows the influence of different tunable parameter combinations on parameters in the stable flow state: as shown in Fig. 9, when the tunable parameter f_g increases, both the riser pressure drop and the inlet pressure decrease accordingly; when the tunable parameter f_l increases, both show an opposite variation trend. In addition, neither f_g nor f_l has an impact on the choke valve pressure drop, because

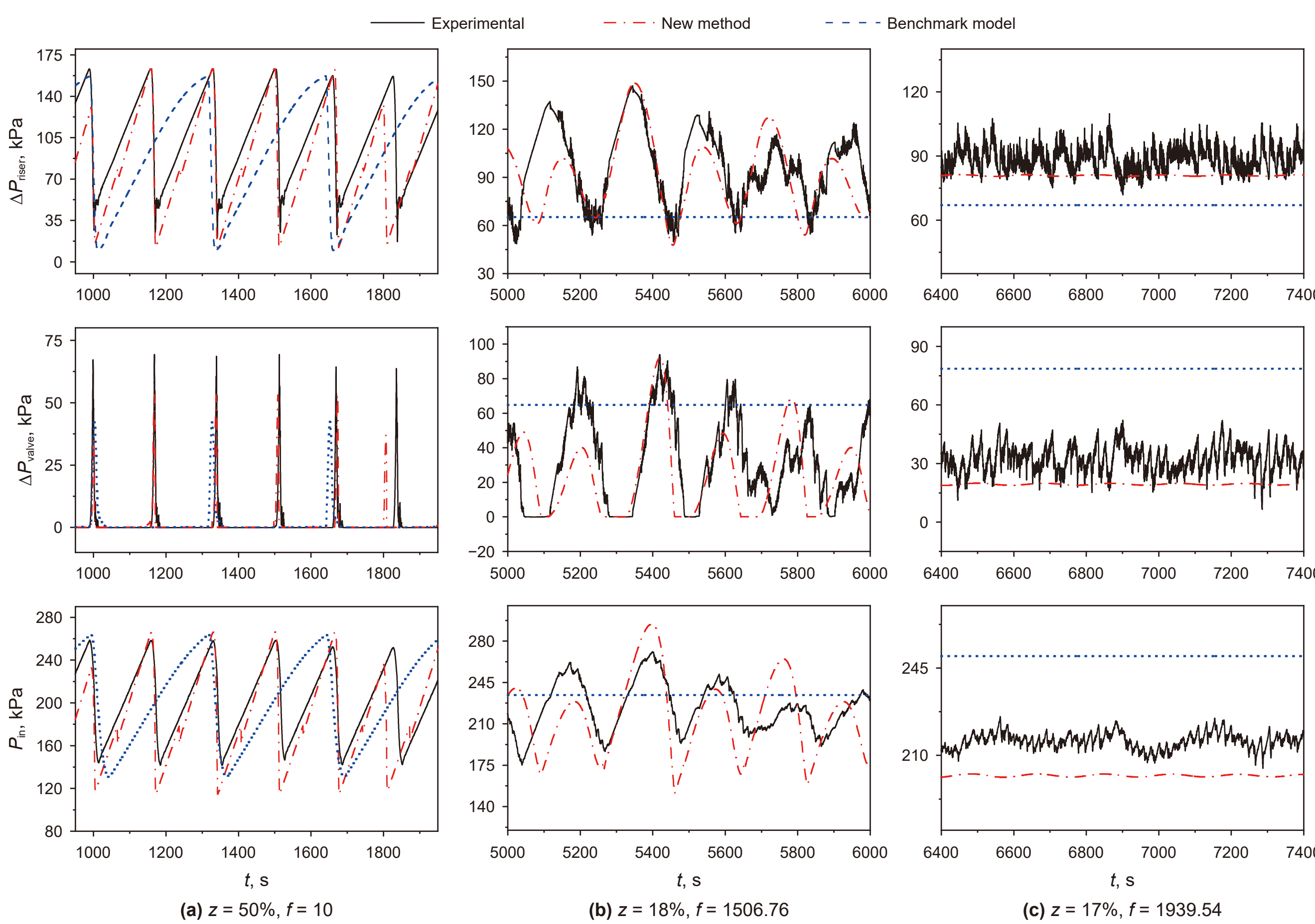

Fig. 12. The micro-display of Case two.

Table 5
Key parameters including slug period of Case one.

	Slug period ($z = 50\%$), s	Slug period ($z = 18\%$), s	ΔP_{riser} ($z = 17\%$), kPa	ΔP_{valve} ($z = 17\%$)	P_{in} ($z = 17\%$)
Experimental results	165.72	201.8	88.61	32.59	215.96
New method	168.3	193.3	84.25	25.9	211.29
Benchmark model	325.1	-	67.28	78.56	249.73

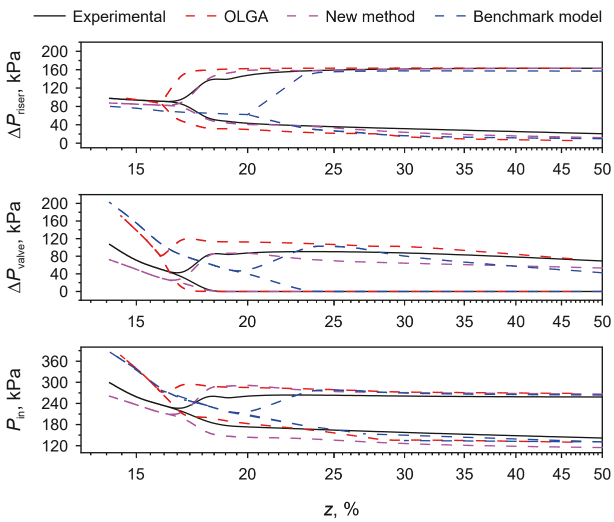

Fig. 13. The bifurcation diagram of Case two.

when the system is stable, the outlet flow rates are consistent with the inlet flow rates, and the choke valve pressure drop will not change significantly when the valve parameters remain unchanged.

4. Results and discussion

Two sets of experimental working conditions and one set of simulated working condition were used to test the simulation performance of the new model. The results will be presented from both macro and micro aspects. The macro-level presentation shows the variation trend of important flow parameters with valve opening and the position of the critical opening in the form of bifurcation diagrams common in active control technique. In the bifurcation diagram, the line with a larger value represents the maximum value of the physical parameter at a certain valve opening, while the line with a smaller value represents the minimum value of this parameter at this opening. As the valve opening decreases, the two lines gradually approach and stick together, indicating that the flow enters a stable state. The opening corresponding to their convergence (bifurcation point) is the critical opening. The micro-level display reveals detailed profiles of flow parameters under different valve openings, such as the wide-open state and the transitional state prior to stabilization as well as immediately after stabilization. The benchmarking adopted here was the Jahanshahi and Skogestad (2011) model. In the final part of this section, this paper also presents the control performance of the simple P controller designed based on the low-dimensional model under the corresponding verification conditions.

4.1. Experimental validation cases

Two representative severe slug flow cases were employed to evaluate the model's performance: Case one represents low gas-liquid ratio conditions (SS1), while Case two corresponds to relatively high gas-liquid ratio conditions (SS2). These two cases exhibit distinct flow characteristics, enabling a comprehensive assessment of the model's predictive accuracy.

The experimental working fluids are water and air, and the parameters involved in the calculation can be found in Table 3.

4.1.1. Case one

For case one, U_{SL} is 0.1 m/s, U_{SG0} is 0.2 m/s; the flow pattern is SS1; its critical opening is 16%, and the corresponding valve resistance coefficient is 2800.56; f_g and fl are equal to 250 and 150 respectively.

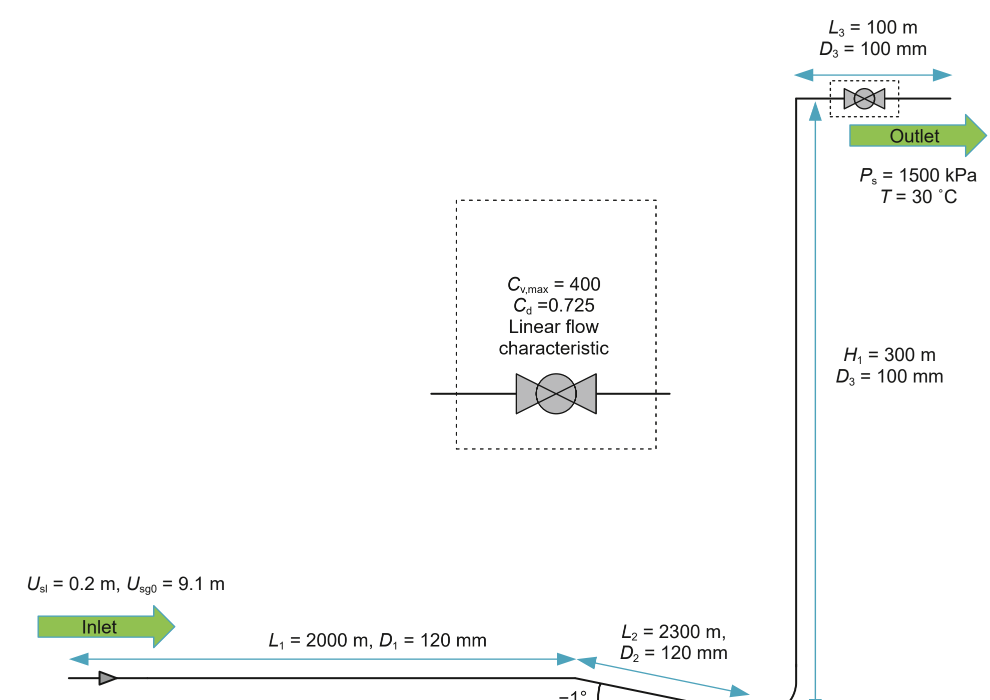

Fig. 14. Schematic diagram of the pipeline system of simulated case.

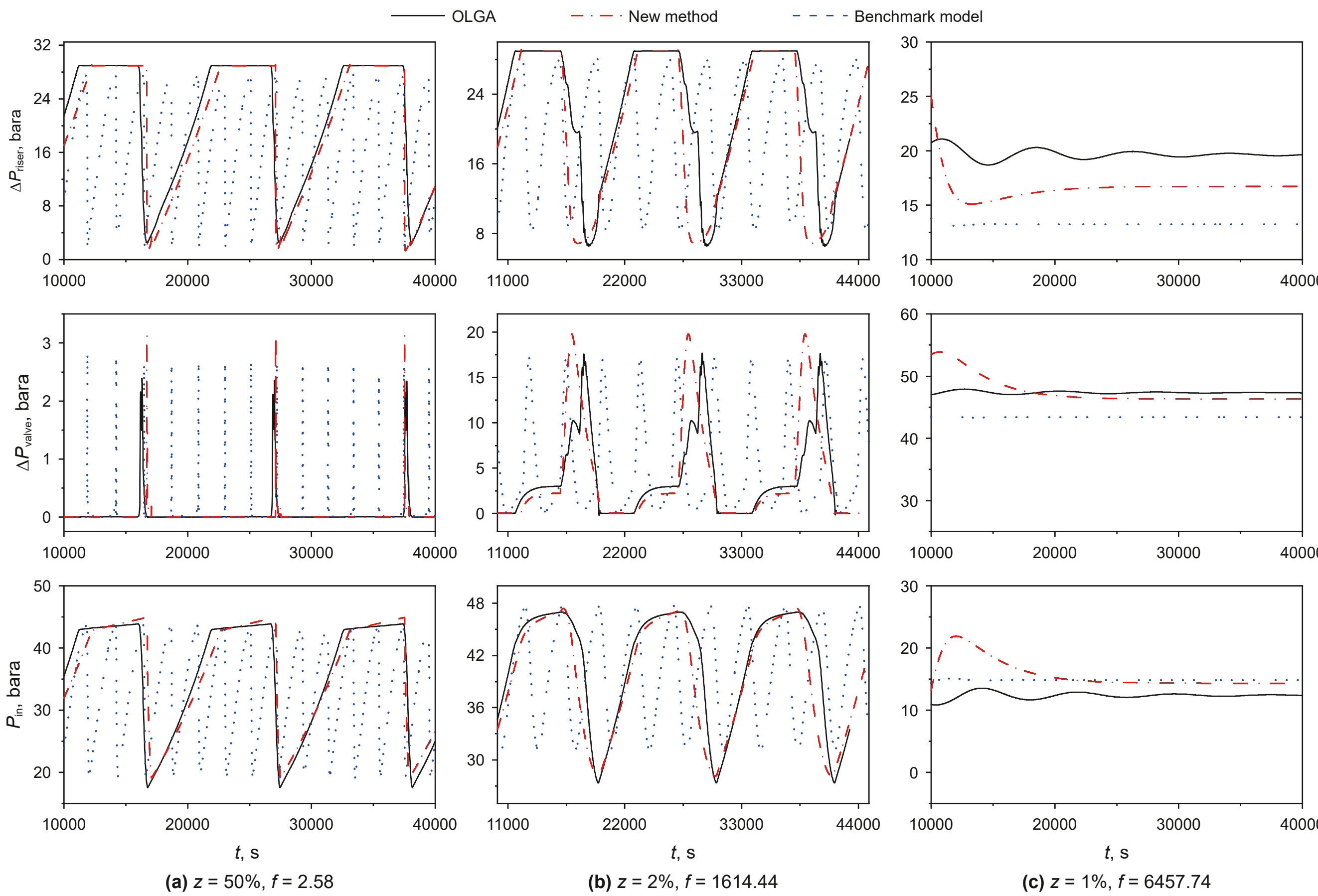

Fig. 15. The micro-display of Simulated case: pressure and pressure drop.

Table 6
Key parameters including slug period of simulated case.

	Slug period ($z = 50\%$), s	Slug period ($z = 2\%$), s	ΔP_{rise} ($z = 1\%$), kPa	ΔP_{valve} ($z = 1\%$), kPa	P_{in} ($z = 1\%$), kPa
OLGA	10694.92	11130	19.66	12.36	47.33
New method	10414.7	11026.65	18.56	13.46	48.11
Benchmark model	2245	3501.65	13.35	14.84	43.4

Fig. 10 presents experimental and simulation data for three key pressure parameters—riser pressure drop (ΔP_{riser}), choke valve pressure drop (ΔP_{valve}), and inlet pressure (P_{in})—across three distinct valve opening positions. As illustrated in Fig. 10, leveraging the refined outlet liquid holdup calculation formula, the proposed model demonstrates enhanced capability in simulating the flow behavior of severe slug flow across various flow stages. Taking the choke valve pressure drop profile in Fig. 10(b) as an example, between 9400 and 9800 s, the flow undergoes a complete process from blowout to slug growth, then to liquid production, and back to blowout. During the slug growth stage, only gas passes through the choke valve. Consequently, the ΔP_{valve} (experimental data, the same below.) is extremely small, approaching zero. In the liquid production stage, the liquid in the riser is slowly accelerated by the gas in the pipeline and pure liquid flows through the choke valve. As a result, the ΔP_{valve} shows a slow-increasing trend, as can be seen from the experimental data around 9600 s. During the blowout stage, gas enters the riser and drives the liquid to flow out of the riser rapidly. Therefore, the ΔP_{valve} rises rapidly and then decreases, entering the next cycle. Similar flow behavior is more obvious in Fig. 15(b). Clearly, the proposed model accurately captures the analogous flow behavior, whereas the benchmark model exhibits some deviations in its simulation results. Within the 9400–9800 s interval, the benchmark model is in slug growth and liquid production stages; however, its ΔP_{valve} remains greater than zero, indicating that there is a huge error in the calculation of the outlet liquid holdup in these two flow stages.

Another example is the riser pressure drop, as shown in Fig. 10(a). Within the time interval of 2000–2200 s, the flow initially belongs to the slug growth stage and subsequently transitions into the liquid production stage. It can be observed that the ΔP_{riser} (experimental data) increases at an almost constant rate, indicating that the flow is in the slug growth stage. Once the full-pipe pressure drop of the riser is reached, the riser pressure drop remains unchanged, as seen around 2200 s. At this point, the flow is in the liquid production stage. The boundaries between these

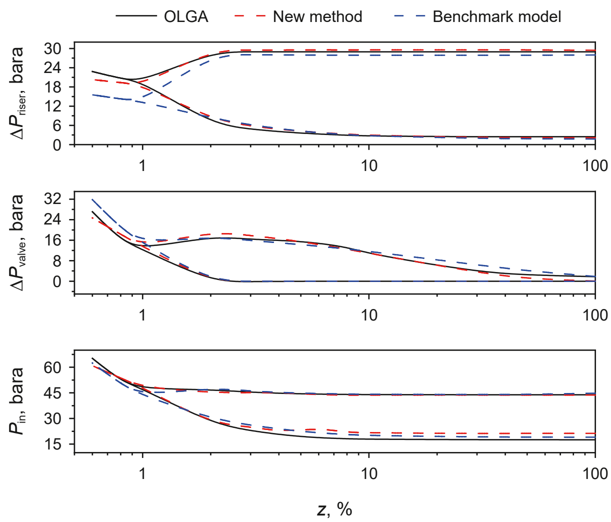

Fig. 16. The bifurcation diagram of Simulated case.

two flow stages are well-defined, enabling researchers to easily distinguish between SS1 and SS2 flow regimes (the former includes the liquid production stage). Unlike the expected trend, the benchmark model predicts a riser pressure drop that rises at a diminishing rate within 1600–2000 s while staying strictly positive.

Moreover, the new model has a better simulation on the cycle than the benchmark model. The specific values are shown in Table 4. This may be caused by the combined changes in the calculation methods of the outlet liquid holdup and the pipeline liquid holdup benchmark model uses the volume liquid holdup instead of the cross-section liquid holdup for calculation, while the proposed model calculates the pipeline liquid holdup based on the cross-section liquid holdup calculation method for horizontal pipe in stratified flow, which is more in line with the study of severe slugging flow.

As depicted in Fig. 11, both models accurately capture the critical opening. Furthermore, the proposed model demonstrates superior predictive performance in simulating the trends of riser pressure drop $\Delta P_{\mathrm{riser}}$, choke valve pressure drop $\Delta P_{\mathrm{valve}}$, and inlet pressure P_{in} across varying valve openings compared to the benchmark model: while both models exhibit a tendency to underestimate the riser pressure drop, the deviation of the proposed model is comparatively smaller. Additionally, the proposed model slightly underestimates the choke valve pressure drop and inlet

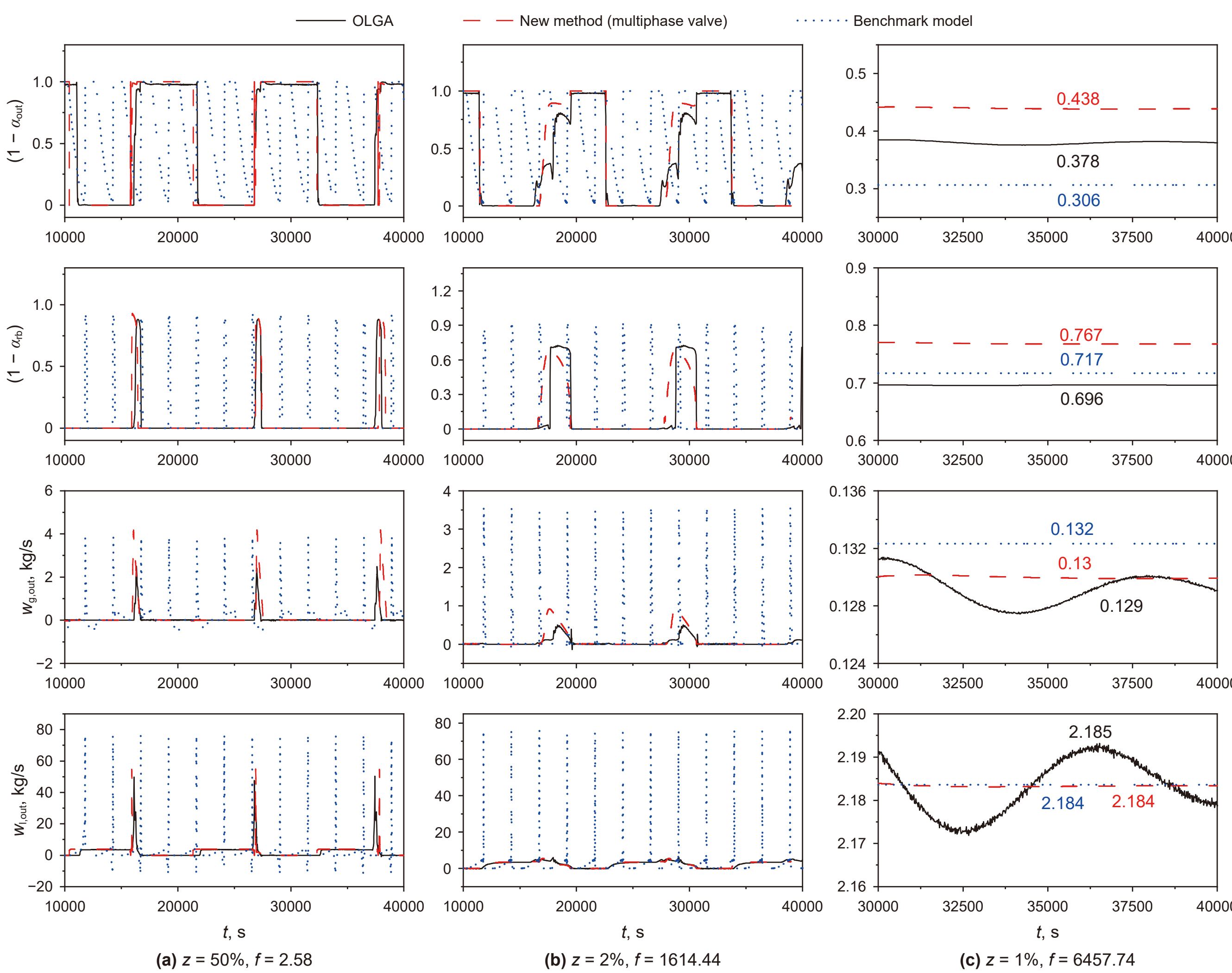

Fig. 17. The micro-display of Simulated case: liquid holdup and outlet mass flow rates.

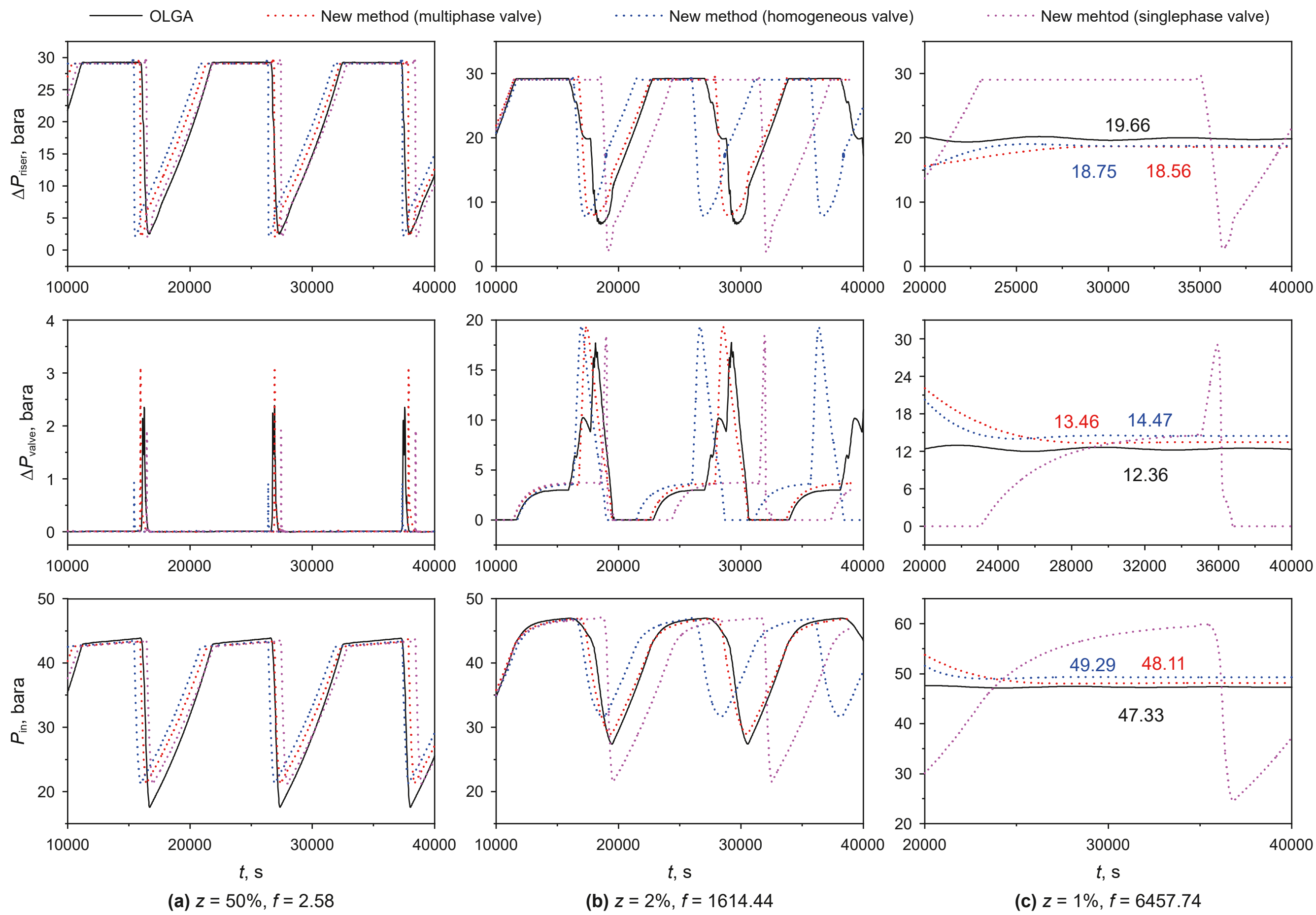

Fig. 18. Demonstration of simulation results of different valve models: pressure and pressure drop.

pressure, whereas the benchmark model overestimates these two parameters.

4.1.2. Case two

For case two, U_{SL} is 0.1 m/s, U_{SG0} is 0.5 m/s; the flow pattern is SS2; its critical opening is 17%, and the corresponding valve resistance coefficient is 1939.54; f_g and f_l are equal to 65 and 55 respectively.

Similar to case one, because the calculation formula of the outlet liquid holdup has a large error in the non-blowout stage, the benchmark model cannot correctly simulate the slug growth stage and the liquid production stage, so it does not have the ability to distinguish between SS1 and SS2, and the SS2 working conditions it simulates are more like the SS1 working conditions with a smaller fluctuation range. As a comparison, the new model can obviously simulate the differences between SS1 and SS2 flow regimes. See the riser pressure drop ΔP_{riser} in Fig. 12(a). Another noteworthy finding is that, during the experimental process, the SS2 working condition exhibited a certain degree of randomness, as evidenced by the lack of complete consistency in the flow profiles across successive cycles, see Fig. 12(b). This variability likely stems from the high gas velocity, which induces randomness in the intensity of each blowout event. Notably, the simulation results of the proposed model also display a comparable degree of stochasticity, as demonstrated in Fig. 12(b) or the 1600–1800 s interval in Fig. 12(a).

In contrast, the simulation results of benchmark model lack this sort of randomness, as shown in Fig. 12(a). Moreover, compared with the proposed model, the existing models exhibit larger periodic errors, as detailed in Table 5.

As shown in Fig. 13, under high gas-liquid ratio conditions, the benchmark model's bifurcation (convergence) point shifts to a significantly larger valve opening. Despite exhaustive parameter tuning by the author, complete agreement between the model and the experiment could not be achieved. This discrepancy suggests that the benchmark model predicts a larger critical opening, translating to a higher flow coefficient under high gas-liquid ratio conditions. Additionally, ΔP_{riser}, choke valve pressure drop ΔP_{valve}, and inlet pressure P_{in}, both models follow trends analogous to Case one.

4.2. Simulation case

4.2.1. Presentation of simulation results

This paper uses OLGA (version 7.0), a commercial software commonly used in industry, to simulate the simple severe slugging flow conditions of large-scale pipeline systems. The pipe size refers to the simulated working condition of Jahanshahi and Skogestad (2011), as shown in Fig. 14, and the working fluid information refers to the working fluid table of Schüller et al. (2006), with only a few modifications. See Appendix B for specific components. The constant information and definitions involved in the calculation are also shown in Appendix B. Only the parameters that are different from those in Table 3 are pointed out in the table. In addition, it should be noted that for this simulated working condition, the multiphase flow valve model is used for calculation, so the constant information involved also includes some thermodynamic parameters of the working fluid.

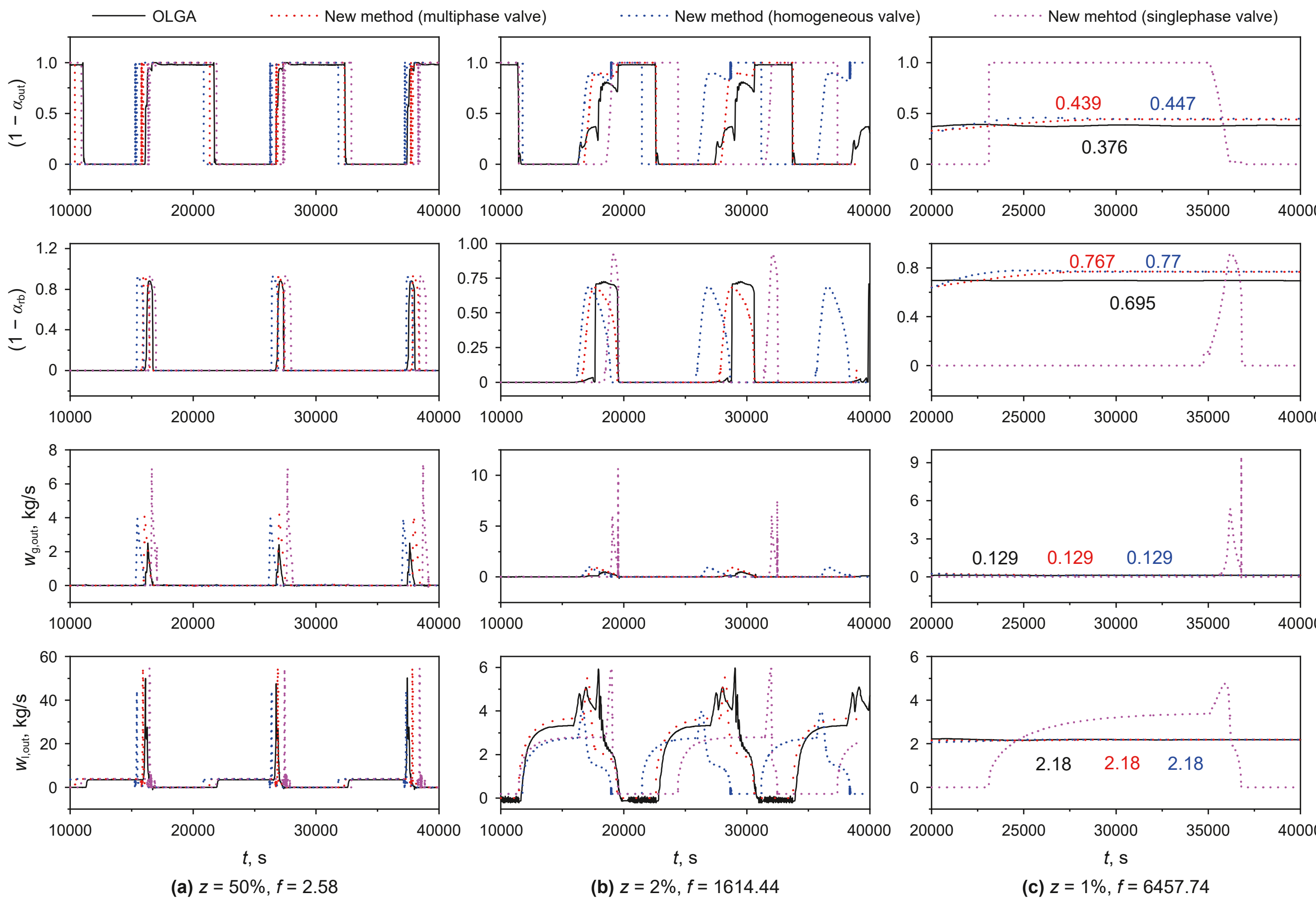

Fig. 19. Demonstration of simulation results of different valve models: void fraction and outlet mass flow rates.

In the simulated case, U_{SG0} is equal to 9.01 m, U_{SL} is 0.2 m, the liquid is an oil-water mixture, and Wc is 90%. When the valve is fully open, the flow coefficient $C_v = 400$, and it satisfies the linear flow characteristic. The critical opening is 1%, and the corresponding resistance coefficient is 6457.74. f_g and f_l are 295 and 150 respectively.

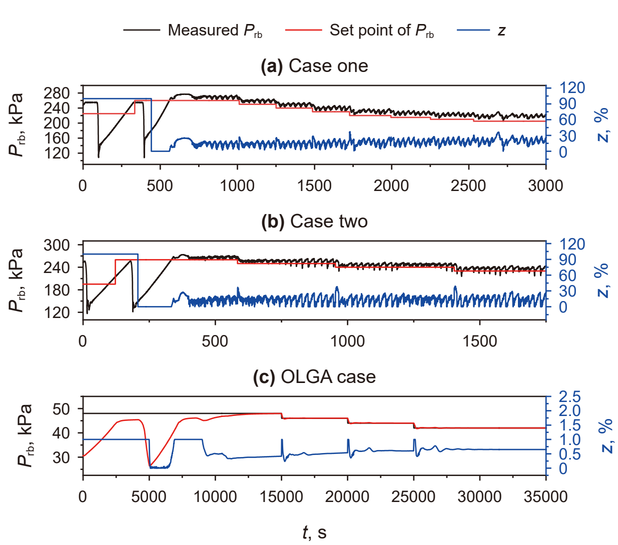

Fig. 20. Presentation of control performance under validation conditions.

As shown in Fig. 15, the multiphase valve model achieves a remarkable enhancement in simulating flow cycle as well as pressure/differential pressure profiles, with precise quantitative data presented in Table 6. Both the new and established models, when relying on the conventional incompressible fluid valve model, invariably underestimate the flow cycle. Moreover, the proposed model outperforms the existing one in simulating inlet pressure P_{in} and riser pressure drop ΔP_{riser} at different valve openings, as depicted in Fig. 16.

With the help of OLGA, it is possible to compare and analyze parameters that are difficult to measure under experimental conditions. This paper selects four parameters for comparative study, namely the outlet liquid phase mass flow rate $w_{l,out}$, outlet gas phase mass flow rate $w_{g,out}$, riser top void fraction 1-α_{out}, and riser base void fraction 1-α_{rb}, and the specific comparison results are shown in Fig. 17. The simulation and comparison results in Fig. 17 further confirm the conclusions drawn in Section 4.1: as shown in (a), when the valve opening is large, the riser top void fraction 1-α_{out} presents a rectangular wave-like variation characteristic, while the benchmark model fails to capture this phenomenon correctly—the calculated riser top void fraction 1-α_{out} decreases to 0 in a relatively gentle trend and then increases rapidly to 1. In addition, by comparing Fig. 17(a) and (b), it can be seen that when the valve opening is large, the severe slugging flow erupts violently, showing a pulsed outlet mass flow rates distribution; as the valve opening decreases, the eruption intensity weakens gradually, and the duration of the blowout stage prolongs, which can be referred to the blowout process before 20000 s in (b) (i.e., the process where the 1-α_{out} increases from 0 to 1). The OLGA software captures more eruption details, and the model in this paper can well reproduce this phenomenon; on the other hand, since the model in this paper can accurately simulate the characteristic of prolonged duration of the blowout stage, it can fit the outlet gas-liquid phase mass flow rates well, and this advantage is more obvious in the comparison of outlet liquid phase mass flow rates in Fig. 19.

4.2.2. Comparison of valve models

Although the homogeneous flow model and the single-phase flow model have achieved good simulation performance under laboratory conditions (Andreolli et al., 2018; Azevedo et al., 2015; Jahanshahi and Skogestad, 2011; Meglio et al., 2009), their application effects in high-pressure working conditions or large-scale pipeline systems remain to be verified. With the help of OLGA validation case, this paper conducts an discussion on the simulation performance of three valve models. Figs. 18 and 19 show the simulation results of the model in this paper using three different valve models, namely the multiphase valve model, the homogeneous valve model, and the single-phase valve model. All tunable parameters remain consistent during the comparison to ensure the objectivity and accuracy of the comparison results.

As shown in Fig. 18(b), when the valve opening is large, the simulation performance of the three valve models are almost identical, with only a certain difference in the outlet gas phase mass flow rate $w_{g,out}$: the single-phase flow model significantly overestimates the $w_{g,out}$. With the increase of the valve's throttling capacity, the differences among the three valve models begin to stand out; among them, the homogeneous valve model and the multiphase valve model show similar variation patterns, both of which can well simulate the variation trend of the blowout stage with the valve opening. The most significant difference between the two is that the multiphase valve model exhibits obvious advantage in the simulation of flow cycles, while the homogeneous valve model underestimates the flow cycles. In addition, the multiphase valve model can better simulate the lower limit of inlet pressure, while the homogeneous valve model overestimates this parameter.

The single-phase flow model has obvious deficiencies in simulation performance: firstly, it cannot accurately simulate the eruption details; secondly, the simulated flow cycle is significantly larger; and the simulation result of the outlet gas phase mass flow rate $w_{g,out}$ is significantly higher, while the simulation result of the lower limit of inlet pressure is significantly lower. It is worth noting that the most prominent problem of the single-phase valve model is poor stability. During the simulation, even if the valve opening is reduced to 0.4%, the flow system cannot be stabilized, and the maximum inlet pressure even reaches 102 bara. This phenomenon indicates that the single-phase valve model significantly underestimates the throttling capacity of the valve.

4.3. Presentation of control performance

For the validation conditions presented in Sections 4.1 and 4.2, this section focuses on presenting the control performance of the simple P controller designed based on the low-dimensional model proposed in this paper. The controller is designed using the criteria given in Park et al. (2021), while the integral part is neglected; during the control process, the riser bottom pressure P_{rb} is selected as the process variable, and the specific control performance are shown in Fig. 20.

5. Conclusions

A low-dimensional model was proposed in this work to break through some possible limitations of the established low-dimensional models and improve their adaptability. The low-dimensional model can be used to study the dynamic process of severe slugging flow in pipeline-riser system, and to design corresponding controllers and estimators. The main conclusions of this paper can be summarized in the following four points.

(1) Based on existing models, a low-dimensional dynamic model containing only two essential tunable parameters is developed. Through in-depth analysis of the flow characteristics of severe slugging, the calculation methods for multiple flow-regime-dependent parameters—such as liquid holdup, flow resistance, and the valve model are discussed and refined. This achieves optimal simulation performance while introducing the minimum number of tunable parameters.
(2) A multiphase valve model that accounts for phase slip is introduced to replace the conventional incompressible flow valve model, thereby significantly improving the model's applicability under actual field conditions. For operating conditions where valve flow may become critical—such as in large-scale, high-pressure pipeline systems—the multiphase valve model can effectively reduce deviations induced by critical flow, thereby enhancing the simulation performance of the low-dimensional dynamic model.
(3) The validation cases include two sets of experimental conditions for two different types of severe slugging flow (i.e., SS1 and SS2) and one set of simulation conditions generated by OLGA. The simulation results are presented in detail to compare the performance of the proposed model with the state-of-the-art low-dimensional model reported in the literature. The proposed model outperforms the benchmark model in terms of the slug cycle, flow behavior, and key flow parameters.
(4) Several future research directions are proposed to improve the model's simulation performance and field applicability, including: developing a slug flow mechanism model with low computational complexity for calculating the riser pressure drop, introducing machine learning methods to improve the calculation accuracy of the outlet liquid holdup, and incorporating the influence of solid particles into the severe slugging flow model.

CRediT authorship contribution statement

Han-Xuan Wang: Writing – original draft, Validation, Software, Methodology, Investigation, Formal analysis, Data curation, Conceptualization. **Tian-Yu Liu:** Investigation, Formal analysis, Data curation. **Sui-Feng Zou:** Writing – review & editing, Supervision, Project administration. **Jie Sun:** Data curation. **Lie-Jin Guo:** Supervision, Resources.

Declaration of competing interest

The authors declare that they have no known competing financial interests or personal relationships that could have appeared to influence the work reported in this paper.

Acknowledgements

This work was financially supported by National Key Research and Development Program of China (No. 2022YFC2806202) and the Fundamental Research Funds for the Central Universities (No. xtr042024002) as well as Central Government Guided Local Science and Technology Development Fund Project (No. 2024ZYD0123).

Appendix A. Multiphase valve model

Under laboratory conditions, the pipeline-riser system is small in scale and low in pressure level. Researchers usually ignore the compressibility of multiphase fluids without proof and use the incompressible flow model to describe the valve, and assume that the valve flow regime is subcritical flow. However, when the attention is shifted to the large-scale and high-pressure on-site working conditions, the above assumptions obviously no longer hold. At this time, the valve model must consider two problems.

(1) The compressibility of multiphase fluids under high pressure introduces new thermodynamic processes;
(2) Whether the flow regime of the valve is sub critical flow or critical flow will affect the pressure drop - flow rate relationship of the valve.

Therefore, a multiphase flow valve model improved based on the Al-safran model (Alsafran and Kelkar, 2007) was added to the low-dimensional model to enhance the simulation performance. More details about this model, including its thermodynamic assumptions, can be found in Shao et al. (2018).

The relationship between valve opening z and throttling orifice diameter D_{valve} is established first. or an orifice plate, the orifice outflow formula gives:

$$Q = C_d A_{\text{valve}} \sqrt{\frac{2\Delta P}{\rho}} \tag{A-1}$$

$$A_{\text{valve}} = 0.25\pi D_{\text{valve}}^2$$

For clarity in the derivation, the symbols and their units are defined as follows: Q is the volumetric flow rate, m^3/s; A_{valve} is the orifice throttling area, m^2; ΔP is the pressure drop across the orifice, Pa; ρ is the fluid density, kg/m^3.

According to the definition of the valve flow coefficient K_v—the volumetric flow rate of water (in m^3/h) that passes through the valve per hour at a pressure drop of 100 kPa across the valve, with water as the fluid (density 1000 kg/m^3, temperature 5-40 °C)—substituting into Eq. (A-1) yields:

$$K_v = 3600 C_d \frac{\pi D_{\text{valve}}^2}{4} \sqrt{\frac{2\times 10^5}{10^3}} \approx 39986 C_d D_{\text{valve}}^2 \tag{A-2}$$

Eq. (A-2) provides a theoretically derived relationship between K_v and D_{valve}, because the true value of C_d is difficult to determine accurately, the actual relationship often deviates from this theoretical expression. To obtain a more precise functional relationship, pure-water experiments should be conducted in accordance with relevant valve standards. Under the assumption of a constant discharge coefficient C_d remains constant, the relationship between z and D_{valve} can then be determined using Eq. (A-1). It should be noted that C_d is actually a parameter that depends on the opening. However, it is usually assumed constant in engineering applications, with all the opening-dependent variations in Eq. (A-1) being incorporated into D_{valve}.

The computational procedure for the multiphase flow valve model is outlined as follows:

Calculate λ and α based on Eqs. (A-3) and (A-4), where υ is specific volume.

$$\lambda = x_{g,\text{out}} \left[k + \frac{1}{Z(k-1)}\right] \tag{A-3}$$

$$\alpha = \upsilon_{g,\text{riser}} \frac{x_{l,\text{out}}}{\rho_l} \tag{A-4}$$

Then calculate the slip ratio S according to Eq. (A-5).

$$S = \sqrt{1 + x_{g,\text{out}}\left(\frac{\upsilon_{g,\text{riser}}}{\upsilon_l} - 1\right)}\left[1 + 0.6e^{-5.0x_{g,\text{out}}}\right] \tag{A-5}$$

Iteratively solve the critical pressure ratio y_c according to Eq. (A-6).

$$\left[2\lambda\left(y_c^{1-1/k} - 1\right) + 2S\alpha(y_c - 1)\right]\left(x_{g,\text{out}} y_c^{-1/k} + \right)\frac{x_{g,\text{out}}}{k} y_c^{-1-1/k} = \left(\lambda\frac{k-1}{k} y_c^{-1/k} + S\alpha\right)\left[r^2\left(x_{g,\text{out}} + S\alpha\right)^2 - \left(x_{g,\text{out}} y_c^{-1/k} + S\alpha\right)^2\right] \tag{A-6}$$

$$r = \frac{A_{\text{valve}}}{A_{\text{riser}}} \tag{A-7}$$

It should be noted that when the liquid holdup α_{out} approaches 1, Eq. (A-6) may not converge. At this time, the properties of multiphase flow are close to those of single-phase liquid. According to Chinese standard GB/T 17213.2 - 2017, the critical pressure ratio of single-phase liquid is estimated by Eq. (A-8). In the formula, P_v and P_c are respectively the absolute pressure of liquid vapor at the inlet temperature and the absolute thermodynamic critical pressure of the liquid. In fact, the critical pressure ratio of single-phase liquid is very small. Therefore, under the working conditions in this paper, it can be considered that the flow regime of the valve at this time is subcritical flow.

$$y_c = 1 - \left(0.96 - 0.28\sqrt{\frac{P_v}{P_c}}\right) \tag{A-8}$$

Then, calculate $P_{2,\text{ valve}}$ and P_3 successively according to Eqs. (A-9) and (A-10), and ignore the possible gas backflow in Eq. (A-10).

$$P_{2,\text{valve}} = P_2 y_c \tag{A-9}$$

$$P_3 = P_2 - \frac{\max(0, P_2 - P_s)}{\left[1 - \left(D_{\text{valve}}/D_{\text{riser}}\right)^{1.885}\right]} \tag{A-10}$$

Judge the numerical magnitudes of the above two pressures to determine the valve flow regime and the actual pressure ratio:

$$\text{flow} = \begin{cases} \text{critical} \quad \text{flow}, & \text{if} \quad P_{2,\text{valve}} \ge P_3 \\ \text{subcritical} \quad \text{flow}, & \text{if} \quad P_{2,\text{valve}} < P_3 \end{cases} \tag{A-11}$$

$$y = \begin{cases} P_{2,\text{valve}}/P_2, & \text{if} \quad P_{2,\text{valve}} \ge P_3 \\ P_3/P_2, & \text{if} \quad P_{2,\text{valve}} < P_3 \end{cases} \tag{A-12}$$

Finally, solve the adiabatic mass flow rate m_a and the final calculated mass flow rate m_c according to Eqs. (A-13) and (A-14). It should be noted that there was a writing error in the calculation formula of m_a in the original literature, and it has been corrected here.

$$m_a^2 = \frac{2P_2 A_{\text{riser}}^2\left[\lambda\left(y^{1-1/k} - 1\right) + S\alpha(y-1)\right]}{\upsilon_{g,\text{riser}}\left(x_{g,\text{out}} + \frac{1}{S}x_{l,\text{out}}\right)\left[r^2\left(x_{g,\text{out}} + S\alpha\right)^2 - \left(x_{g,\text{out}} y^{-1/k} + S\alpha\right)^2\right]} \tag{A-13}$$

$$m_c = C_d m_a \tag{A-14}$$

All constants involved in the calculations in Appendix A, their value and definitions are shown in Appendix B.

Appendix B. Details about simulation

The PVTfile required for OLGA simulation are generated by commercial software. The working fluids information is modeled after that of Schüller et al. (2006), with only minor modifications. The specific proportions are shown in Table B-1. The constants involved in the calculation, their definitions and values are shown in Table B-2. The parameters in Table B-2 are obtained from the working medium information generated by commercial software. The temperature condition is 30 °C, and the pressure condition is the sum of the separator pressure and the full-hydraulic drop of the riser.

Table B-1
Working fluids components table.

	Gas phase, mol%	Oil phase, mol%	Water phase, mol%
Nitrogen	1.56	0.02	0.00
Carbon dioxide	0.79	0.06	0.00
Methane	84.38	3.47	0.00
Ethane	7.63	1.47	0.00
Propane	2.38	1.40	0.00
Iso-butane	0.52	0.66	0.00
Butane	1.41	2.54	0.00
Iso-pentane	0.41	1.63	0.00
Pentane	0.48	2.51	0.00
C6+	0.44	86.24	0.00
Nacl	0.00	0.00	0.01
Water	0.00	0.00	99.99

Table B-2
The values and definitions of the calculation constants.

Symbol	Description	Value	Unit
M	Gas molecular	19.81e-3	kg/mol
T	Temperature	303.15	K
Z	Compressibility factor	0.9006	·
μ_l	Liquid viscosity	0.2903e-3	Pa·s
μ_g	Gas viscosity	0.0122e-3	Pa·s
ε	Pipe roughness	2.8e-5	m
ρ_o	Oil density	624.89	kg/m^3
ρ_{g0}	Gas density under standard conditions	1.275	kg/m^3
ρ_l	Liquid density	965.23	kg/m^3
W_c	Water cut	0.9	·
GOR	Gas-Oil ratio	454.52	·
GLR	Gas-Liquid ratio	45.04	·
U_{SL}	Liquid superficial velocity	0.2	m/s
U_{SG0}	Gas superficial velocity under standard conditions	9.01	m/s
C_{vg}	Specific heat value of gas at constant volume condition	46.97	J/(mol·K)
C_{pg}	Specific heat value of gas at constant pressure condition	32.96	J/(mol·K)
k	Ratio of specific heat (C_{pg}/C_{vg})	1.425	·
$C_{v,max}$	Valve flow coefficient Cv at fully open	400	m^3/h
C_d	Valve discharge coefficient at fully open	0.725	·

References

Alsafran, E.M., Kelkar, M.G., 2007. Predictions of two-phase critical flow boundary and mass flow rate across chokes. In: SPE Annual Technical Conference and Exhibition, Richardson. Society of Petroleum Engineers. SPE 109243–MS. https://doi.org/10.2118/109243-ms.

Andreolli, I., de Azevedo, G.R., Baliño, J.L., 2018. Stability solver for offshore oil production systems. J. Petrol. Sci. Eng. 171, 993–1006. https://doi.org/10.1016/j.petrol.2018.08.013.

Azevedo, G.R., Baliño, J.L., Burr, K.P., 2015. Linear stability analysis for severe slugging in air–water systems considering different mitigation mechanisms. Int. J. Multiphas. Flow 73, 238–250. https://doi.org/10.1016/j.ijmultiphaseflow.2015.03.021.

Azevedo, G.R., Baliño, J.L., Burr, K.P., 2017. Influence of pipeline modeling in stability analysis for severe slugging. Chem. Eng. Sci. 161, 1–13. https://doi.org/10.1016/j.ces.2016.12.004.

Baliño, J.L., Burr, K.P., Nemoto, R.H., 2010. Modeling and simulation of severe slugging in air–water pipeline–riser systems. Int. J. Multiphas. Flow 36 (8), 643–660. https://doi.org/10.1016/j.ijmultiphaseflow.2010.04.003.

Banjara, V., Pereyra, E., Avila, C., et al., 2023. Critical review & comparison of severe slugging mitigation techniques. Geoenergy Sci. Eng. 228, 212082. https://doi.org/10.1016/j.geoen.2023.212082.

Cao, Y., Xu, Q., Yu, H., et al., 2024. Experimental investigation and prediction of overall and local flow patterns in pipeline-riser systems. Int. J. Multiphas. Flow 175, 104794. https://doi.org/10.1016/j.ijmultiphaseflow.2024.104794.

Chen, S., Zeng, L., Zhang, Z., et al., 2025. Progress and outlook on severe slugging mitigation techniques for offshore hydrocarbon production: a systematic review. Geoenergy Sci. Eng. 246, 213546. https://doi.org/10.1016/j.geoen.2024.213546.

Colebrook, C.F., 1939. Turbulent flow in pipes, with particular reference to the transition region between the smooth and rough pipe laws. J. Inst. Civ. Eng. 11 (4), 133–156. https://doi.org/10.1680/ijoti.1939.13150.

Haaland, S.E., 1983. Simple and explicit formulas for the friction factor in turbulent pipe flow. J. Fluid Eng. 105 (1), 89–90. https://doi.org/10.1115/1.3240948.

Han, P., Guo, L., 2015. Numerical simulation of terrain-induced severe slugging coupled by hydrodynamic slugs in a pipeline–riser system. Int. J. Heat Fluid Flow 56, 355–366. https://doi.org/10.1016/j.ijheatfluidflow.2015.10.005.

Havre, K., Dalsmo, M., 2002. Active feedback control as a solution to severe slugging. SPE Prod. Facil. 17 (3), 138–148. https://doi.org/10.2118/79252-pa.

Havre, K., Stornes, K.O., Stray, H., 2000. Taming slug flow in pipelines. Pipes Pipelines Int. 46, 23–30. https://search.abb.com/library/Download.aspxDocumentID=100580A1337.

Jahanshahi, E., De Oliveira, V., Grimholt, C., et al., 2014. A comparison between internal Model Control, optimal PIDF and robust controllers for unstable flow in risers. IFAC Proc. Vol. 47 (3), 5752–5759. https://doi.org/10.3182/20140824-6-ZA-1003.02381.

Jahanshahi, E., Skogestad, S., 2011. Simplified dynamical models for control of severe slugging in multiphase risers. IFAC Proc. Vol. 44 (1), 1634–1639. https://doi.org/10.3182/20110828-6-IT-1002.00981.

Jansen, F.E., Shoham, O., Taitel, Y., 1996. The elimination of severe slugging: experiments and modeling. Int. J. Multiphas. Flow 22 (6), 1055–1072. https://doi.org/10.1016/0301-9322(96)00027-4.

Kaasa, G.O., Alstad, V., Zhou, J., et al., 2008. Attenuation of slugging in unstable oil wells by nonlinear control. IFAC Proc. Vol. 41 (2), 6251–6256. https://doi.org/10.3182/20080706-5-KR-1001.01055.

Li, W., Guo, L., Xie, X., 2017. Effects of a long pipeline on severe slugging in an S-shaped riser. Chem. Eng. Sci. 171, 379–390. https://doi.org/10.1016/j.ces.2017.05.017.

Liu, T., Zou, S., Wang, H., et al., 2025. Cyclic flow cut-off characteristics of gas-liquid two-phase flow in pipeline-riser system and prediction of its occurring condition. Int. J. Multiphas. Flow 182, 105042. https://doi.org/10.1016/j.ijmultiphaseflow.2024.105042.

Liu, Z., Liao, R., Lei, Y., et al., 2019. Pressure drop model of oil-gas two-phase flow in horizontal pipes with different diameters. Sci. Technol. Eng. 19 (34), 137–143. https://doi.org/10.3969/j.issn.1671-1815.2019.34.019 (in chinese).

Malekzadeh, R., Henkes, R.A.W.M., Mudde, R.F., 2012. Severe slugging in a long pipeline–riser system: experiments and predictions. Int. J. Multiphas. Flow 46, 9–21. https://doi.org/10.1016/j.ijmultiphaseflow.2012.06.004.

Martins, Da Silva C., Dessen, F., Nydal, O.J., 2010. Dynamic multiphase flow models for control, 7th north American conference on multiphase technology. In: 7th North American Conference on Multiphase Technology. https://onepetro.org/BHRNACMT/proceedings-abstract/BHR10/BHR10/BHR-2010-F2/155.

Meglio, F.D., Kaasa, G.O., Petit, N., 2009. A first principle model for multiphase slugging flow in vertical risers. In: Proceedings of the 48h IEEE Conference on Decision and Control (CDC) Held Jointly with 2009 28th Chinese Control Conference, pp. 8244–8251. https://doi.org/10.1109/CDC.2009.5400680.

Nemoto, R.H., Baliño, J.L., 2012. Modeling and simulation of severe slugging with mass transfer effects. Int. J. Multiphas. Flow 40, 144–157. https://doi.org/10.1016/j.ijmultiphaseflow.2011.11.005.

Nnabuife, S.G., Tandoh, H., Whidborne, J.F., 2022. Slug flow control using topside measurements: a review. Chem. Eng. J. Adv. 9, 100204. https://doi.org/10.1016/j.ceja.2021.100204.

Ogazi, A.I.I., Cao, Y., Yeung, H., et al., 2010. Slug control with large valve openings to maximize oil production. SPE J. 15 (3), 812–821. https://doi.org/10.2118/124883-pa.

Park, K.H., Kim, T.W., Kim, Y.J., et al., 2021. Experimental investigation of model-based IMC control of severe slugging. J. Petrol. Sci. Eng. 204, 108732. https://doi.org/10.1016/j.petrol.2021.108732.

Pedersen, S., Durdevic, P., Yang, Z., 2017. Challenges in slug modeling and control for offshore oil and gas productions: a review study. Int. J. Multiphas. Flow 88, 270–284. https://doi.org/10.1016/j.ijmultiphaseflow.2016.07.018.

Schüller, R.B., Munaweera, S., Selmer-Olsen, S., et al., 2006. Critical and sub-critical oil/gas/water mass flow rate experiments and predictions for chokes. SPE Prod. Oper. 21 (3), 372–380. https://doi.org/10.2118/88813-pa.

Shao, H., Jiang, L., Liu, L., et al., 2018. Modeling of multiphase flow through chokes. Flow Meas. Instrum. 60, 44–50. https://doi.org/10.1016/j.flowmeasinst.2018.02.015.

Storkaas, E., Skogestad, S., 2003. A low-dimensional Dynamic Model of Severe Slugging for Control Design and Analysis. https://www.semanticscholar.org/paper/A-low-dimensional-dynamic-model-of-severe-slugging-Storkaas-Skogestad/25968aacc081415ad20df0ea10996495e71ae089.

Taitel, Y., 1986. Stability of severe slugging. Int. J. Multiphas. Flow 12 (2), 203–217. https://doi.org/10.1016/0301-9322(86)90026-1.

Taitel, Y., Dukler, A.E., 1976. A model for predicting flow regime transitions in horizontal and near horizontal gas-liquid flow. AIChE Journal 22 (1), 47–55. https://doi.org/10.1002/aic.690220105.

Taitel, Y., Vierkandt, S., Shoham, O., et al., 1990. Severe slugging in a riser system: experiments and modeling. Int. J. Multiphas. Flow 16 (1), 57–68. https://doi.org/10.1016/0301-9322(90)90037-J.

Wang, C., Chen, L., Li, L., et al., 2023. Combining unscented Kalman filter and wavelet neural network for anti-slug. Pet. Sci. 20 (6), 3752–3765. https://doi.org/10.1016/j.petsci.2023.05.008.

Wang, H.X., Xu, L.H., Zou, S.F., et al., 2026. Estimation model of critical opening of topside choking for slugging elimination in pipeline-riser system. Chem. Eng. Sci. 321, 122810. https://doi.org/10.1016/j.ces.2025.122810.

Wang, H., Zou, S., Liu, T., et al., 2024. Experimental investigation of online solving for critical valve opening for eliminating severe slugging in pipeline-riser systems. Int. J. Heat Fluid Flow 110, 109584. https://doi.org/10.1016/j.ijheatfluidflow.2024.109584.

Xie, C., Guo, L., Li, W., et al., 2017. The influence of backpressure on severe slugging in multiphase flow pipeline-riser systems. Chem. Eng. Sci. 163, 68–82. https://doi.org/10.1016/j.ces.2017.01.028.

Yu, H.Y., Xu, Q., Cao, Y.Q., et al., 2023. Characterizations of gas-liquid interface distribution and slug evolution in a vertical pipe. Pet. Sci. 20 (5), 3157–3171. https://doi.org/10.1016/j.petsci.2023.03.009.

Yu, H., Xu, Q., Huang, B., et al., 2024. A visualization study on characteristics of severe slugging in the S-shaped riser with a kilometer-scale pipeline. Exp. Therm. Fluid Sci. 155, 111175. https://doi.org/10.1016/j.expthermflusci.2024.111175.

Zhao, X., Xu, Q., Wu, Q., et al., 2023. Effect of high pressure on severe slugging and multiphase flow pattern transition in a long pipeline-riser system. Exp. Therm. Fluid Sci. 148, 110976. https://doi.org/10.1016/j.expthermflusci.2023.110976.

Zhou, H., Guo, L., Yan, H., et al., 2018. Investigation and prediction of severe slugging frequency in pipeline-riser systems. Chem. Eng. Sci. 184, 72–84. https://doi.org/10.1016/j.ces.2018.03.050.

Zou, S., Guo, L., Xie, C., 2017. Fast recognition of global flow regime in pipeline-riser system by spatial correlation of differential pressures. Int. J. Multiphas. Flow 88, 222–237. https://doi.org/10.1016/j.ijmultiphaseflow.2016.08.007.

Zhou, Y., Sun, B., Liang, Q., et al., 2002. The prediction of liquid layer height and calculation of void fraction on gas-liquid stratified flow in inclined downward tubes. J. Eng. Thermophys. 23, 238–240. https://doi.org/10.3321/j.issn:0253-231X.2002.02.031 (in Chinese).

Zou, S., Guo, L., Yao, T., 2021. Upstream-flow-based mechanisms for global flow regime transition of gas/liquid two-phase flow in pipeline-riser systems. Chem. Eng. Sci. 240, 116542. https://doi.org/10.1016/j.ces.2021.116542.